Available online at www.sciencedirect.com
SCIENCE DIRECT®
Nuclear Instruments and Methods in Physics Research A 499 (2003) 280–315
NUCLEAR INSTRUMENTS & METHODS IN PHYSICS RESEARCH Section A
www.elsevier.com/locate/nima

The RHIC magnet system

M. Anerella, J. Cottingham, J. Cozzolino, P. Dahl, Y. Elisman, J. Escallier, H. Foelsche, G. Ganetis, M. Garber, A. Ghosh, C. Goodzeit, A. Greene, R. Gupta, M. Harrison, J. Herrera, A. Jain, S. Kahn, E. Kelly, E. Killian, M. Lindner, W. Louie, A. Marone, G. Morgan, A. Morgillo, S. Mulhall, J. Muratore, S. Plate, A. Prodell, M. Rehak, E. Rohrer, W. Sampson, J. Schmalzle, W. Schneider, R. Shutt, G. Sintchak, J. Skaritka, R. Thomas, P. Thompson, P. Wanderer*, E. Willen

Brookhaven National Laboratory, Upton, NY 11973, USA

Abstract

The magnet system of the collider consists of superconducting dipole, quadrupole and correction magnets for guiding and focusing the beams through the regular arcs of the machine lattice as well as into collision at the six interaction points. It is designed to allow operation in the energy range 30–100 GeV/u. Operation with either equal or unequal ion species in the colliding beams is possible, imposing a ratio of up to 2.5:1 in the magnetic fields of the two rings. There are 1740 superconducting magnets in the machine. They were designed to meet stringent requirements on field quality, reproducibility, and long-term reliability while being inexpensive to produce. Wherever feasible, production of magnets and components was carried out in industry, always with build-to-print designs. After several years of operation, no magnet has failed and the magnet system has proven reliable and functional.
© 2002 Elsevier Science B.V. All rights reserved.

Keywords: Accelerator magnets; Superconducting magnets; Helical magnets; RHIC magnets; Magnet field quality

1. Introduction

The magnet system of the collider consists of superconducting dipole, quadrupole and correction magnets for guiding and focusing the beams through the regular arcs of the machine lattice as well as into collision at the six interaction points. It is designed to allow operation in the energy range 30–100 GeV/u corresponding to a Bρ of 97–840 T m. Operation with either equal or unequal ion species in the colliding beams is possible, imposing a ratio of up to 2.5:1 in the magnetic fields of the two rings.

Besides reaching fields with substantial margins above the required field range, all of the RHIC magnets meet stringent requirements on field quality, reproducibility, and long-term reliability. Basic designs were chosen early based on technical superiority combined with the prospect of low cost production [1,2]. Starting with existing technology,

*Corresponding author. Tel.: +1-631-344-7687; fax: +1-631-344-2190.
E-mail address: wanderer@bnl.gov (P. Wanderer).

0168-9002/03/$ - see front matter © 2002 Elsevier Science B.V. All rights reserved.
doi:10.1016/S0168-9002(02)01940-X

many new methods were adopted for the magnet design and construction, measuring and analysis procedures, cooling method, quench protection, instrumentation, and quality control. These methods were developed and tested in an R&D phase and were incorporated into designs and fabrication methods as warranted. Wherever practicable, series production of magnets was then carried out in industry following prints and production methods developed at Brookhaven in the R&D phase. This combination of proven, cost-efficient design and industrial production resulted in reliable magnets and modest, well-controlled magnet costs [3]. Several papers summarize the status of the magnet program as it proceeded [4,5].

The RHIC magnet lattice was designed to fit into the existing tunnel of ~3.8 km circumference. The lattice is divided into 6 arcs and 6 insertions for each of the two rings. In the arcs, the rings are separated radially by 90 cm. Table 1 gives the RHIC magnet inventory and several magnet size parameters. Magnets with a coil inner diameter of 80 mm are referred to as "standard aperture" magnets.

Table 1
RHIC magnet inventory and basic parameters

Magnet	Number	Coil diameter (mm)	Length (m)
Dipoles			
Arc	264	80	9.45
D5I, D5O	12, 12	80	6.92, 8.71
D6, D8, D9	24, 24, 24	80	2.95, 9.45, 2.95
D0	24	100	3.6
DX	12	180	3.7
Quadrupoles			
Arc	276	80	1.13
Q4, Q5, Q6	24, 24, 24	80	1.83, 1.13, 1.13
Q7, Q8, Q9	24, 24, 24	80	0.95, 1.13, 1.13
Q1, Q2, Q3	24, 24, 24	130	1.44, 3.40, 2.10
Sextupoles			
Arc, Q9	276, 12	80	0.75
Trim Quadrupoles			
Q4, Q5, Q6	24, 24, 24	80	0.75
Correctors			
B, C, D, E, F	96, 132, 78, 78, 36	80	0.5
I, J, K, L, M	12, 12, 24, 12, 12	130	0.5

2. Superconductor

2.1. Superconducting wire for cable

A 30-strand superconducting cable was used in the fabrication of all of the dipole and quadrupole magnets with 80 and 100 mm apertures [6,7]. For the 130 and 180 mm magnets, a 36-strand cable was used. The properties of the NbTi superconducting wire used to fabricate these cables are summarized in Table 2. It was manufactured by Oxford Superconducting Technology, Carteret, NJ (wire for the Q3 quadrupoles was manufactured by The Furukawa Electric Co., Tokyo, Japan). The small filament diameter of 6 μm was chosen to minimize deleterious time-dependent effects [8] in machine operation [9].

The wire minimum critical current is defined at a temperature of 4.22 K, an applied magnetic field of 5 T (5.6 T for 36-strand cable wire) perpendicular to the wire axis and a resistivity of $1 \times 10^{-14}\,\Omega\,\mathrm{m}$ based on the total wire cross-section. This current requirement corresponds to a minimum current density in the NbTi superconductor of $2600\,\mathrm{A/mm^2}$ at 5 T ($2420\,\mathrm{A/mm^2}$ at 5.6 T, or $2750\,\mathrm{A/mm^2}$ at 5 T, for 36-strand cable wire). Such modest goals were chosen for the RHIC magnets because higher values were unnecessary to meet the accelerator

Table 2
Parameters of superconducting wire used in cable for RHIC magnets

Parameter	Value (30-strand cable)	Value (36-strand cable)
Wire diameter (mm)	0.648	0.648
Filament diameter (μm)	6	6
Copper/non-copper ratio	2.25/1	1.80/1
Number of filaments	3510	4150
Min. crit. curr., 5 T, 4.22 K (A)	264	
Min. crit. curr., 5.6 T, 4.22 K (A)		286
Min. RRR	38	36

design objectives, and because the emphasis for superconductor manufacturing was placed on uniformity of wire and cable properties. In manufacturing, about 2800 A/mm^2 was achieved for the 30-strand cable wire. An upper limit was placed on wire critical current at 3.0 T in order to control the effects of superconductor magnetization at injection. The relatively high proportion of copper in the strand was chosen to add stability against quenching and to lower peak temperatures during a quench.

2.2. Superconducting cable

The properties of the Rutherford-type cables are given in Table 3. The variations of the cable dimensions, especially the cable mid-thickness, were tightly controlled because the magnetic field quality of the magnets and the coil prestress were strongly dependent on them. The cable lay (or twist) pitch was chosen to be opposite to the wire twist and required a cabler operating in a planetary mode for fabrication. In this mode, the wire twist is preserved during cabling. The cable minimum critical current (see Table 3) is defined in a way similar to that for the wire, but with the magnetic field perpendicular to the wide surface of the cable and with compensation for self-field. All cable lengths were produced without cold welds. It was manufactured by New England Electric Wire Corporation, Lisbon, NH. (Cable for Q3 quadrupoles was manufactured by The Furukawa Electric Co., Tokyo, Japan.)

Table 3
Parameters of superconducting cable used for RHIC magnets

Parameter	Value (30-strand cable)	Value (36-strand cable)
No. of wires in cable	30	36
Mid-thickness (mm)	1.166	1.156
Width (mm)	9.73	11.68
Keystone angle (degrees)	1.2	1.0 (130 mm quads) 0.6 (180 mm dipoles)
Min. crit. curr., 5 T, 4.2 K (A)	7524	
Min. crit. curr., 5.6 T, 4.2 K (A)		10,100

Table 4
Parameters of superconducting wire used for RHIC sextupole, trim quadrupole and corrector magnets

Parameter	Value (sext, trim quad)	Value (corrector)
Wire diameter (mm)	0.508	0.330
Filament diameter (μm)	10	10
Copper/non-copper ratio	3/1	2.5/1
Number of filaments	645	310
Min. crit. Curr., 2 T, 4.2 K (A)	230	120
Min. RRR	90	90

2.3. Sextupole, trim quadrupole and corrector wire

The wire used to fabricate coils for the sextupole and trim quads was all the same and a similar but smaller diameter wire was used for the corrector magnets. Since these coils are wound from wire, not from cable, the integrity and uniformity of the wire along the length is critical for the operation of the magnets. The magnets and superconductor were designed with considerable margin between the expected operating current and the critical current, to add reliability. The properties of the superconducting wires for these magnets are summarized in Table 4. The nominal filament diameter of 10 μm is somewhat larger than that for cable magnets, reflecting a reduced concern about magnetization effects in these magnets. This wire was manufactured by The Furukawa Electric Co., Tokyo, Japan, using a continuous annealing process.

3. Standard aperture dipoles

3.1. Cold mass

The arc dipole magnets represent by far the largest single cost item for the collider. Following extensive R&D [10,11], they were manufactured by Northrop Grumman Corporation, Bethpage, NY as a build-to-print design. Fig. 1 shows a cross-section of the cold mass, which is the central inner structure that produces the field and that contains the cold helium. The design is based on a relatively large bore (80 mm inner diameter), single-layer

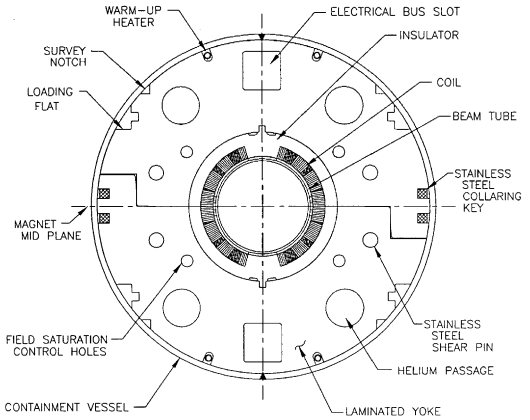

Fig. 1. Cross-section of the arc dipole magnet.

Table 5
Selected parameters of the arc dipole magnet

Parameter		Value
Field (T)	at injection	0.401
	at top energy	3.458
Current (A)	at injection	568
	at top energy	5050
Magnet rigidity (T m)	at injection	97.5
	at top energy	839.5
Magnetic length (m)		9.45
Cold mass length (m)		9.73
Magnet bending radius, cold (m)		243
Mechanical sagitta (mm)		48.5
Cold mass weight (kg)		3607
Inductance (mH)		28
Stored energy (kJ)		351

"cosine theta" coil, wound from the (partially) keystoned, 30-strand cable described earlier, and mechanically supported by a laminated, cold steel yoke encased in a stainless steel shell. The shell contains the helium and is also a load bearing part of the assembly. This cold mass assembly is mounted within a cryostat consisting of a cylindrical vacuum vessel, an aluminum heat shield, blankets of multilayer thermal insulation, cryogenic headers, and the magnet support system. The nominal dipole operating field is 3.458 T at a current of 5.050 kA and an operating temperature between 4.3 and 4.6 K. The general design parameters are listed in Table 5.

3.2. Coil

The superconducting coil was assembled from two half-coils that were wound on automated machinery and then formed into a specified size in a precision molding operation. Each half-coil consists of a single layer of 32 turns arranged in four blocks with three intervening symmetric copper wedges; the sizes and positions of the wedges and the coil pole spacer were designed to result in field harmonics meeting the rigid field quality specifications required for RHIC. The cable length per half-coil is 1220 m. This cable was insulated with 2 double layers of newly developed Kapton CI film [12]. The first double layer has polyimide adhesive on the outer side of the tape; the second has it on both sides. This marked the first use of all-polyimide electrical insulation in the coils of superconducting accelerator magnets, an advance that has greatly improved their electrical integrity. It has also reduced size variations in molded coils, leading directly to improved magnet field quality. The coil ends were designed for relatively simple construction and low harmonic content [13,14]. There are 8 (9) separate spacers in the lead (return) end of each coil, molded of Ultem 6200 plastic. The coils were keyed to the yoke laminations through the precision-molded, glass-filled phenolic (RX630) insulator-spacers. The phenolic insulators separate the coil from the steel yoke and provide both electrical isolation of the coil from ground as well as reduced magnetic saturation effects at high field. The coil design used sufficiently thick midplane caps to allow adjustment of sextupole and decapole harmonics during production [15].

3.3. Beam tube

The dipole utilizes a cold beam tube with an outer diameter of 73 mm and a wall thickness of 1.96 mm. It is centered horizontally inside the coils with attached G-10 longitudinal bumpers and vertically by the insulator poles. This defines a radial helium buffer space of 3.4 mm, which is needed to permit adequate cooling helium flow through the magnet and to reduce quench pressures in the magnets [16]. It is wrapped with

Kapton insulation to provide electrical isolation of the coil from ground potential. The tube is made of seamless, type 316 LN stainless steel, manufactured by Mannesmann Edelstahlrohr, Germany in accordance with the chemical composition requirements of the ASTM A213/A231M specification, but with a nickel content toward the upper part of the allowable range to mitigate potential welding problems at the ends of the tubes. No copper coating on the tube inner surface was required in the RHIC machine. The beam tubes were welded to the end volumes at each end of the magnet, with no intervening bellows.

3.4. Yoke

The steel yoke performs several functions: it serves as a magnetic return path and thereby enhances the central field, it acts as a "collar" that applies mechanical prestress to the coils through the phenolic insulator-spacer that references the coils to the yoke, and finally, it acts as a shield to reduce stray field in the adjacent ring of magnets. The yoke laminations contain holes for the necessary busses and for the flow of helium. The sizes and positions of these holes, and of the locating notch for the RX630 spacers, were carefully determined to minimize saturation effects [15]. Special strain gauge instrumentation and test methods were developed to ensure that the stresses in the magnet met the design goals [17]. Using the yoke laminations as collars dictated the lamination thickness. The magnetic uniformity of the steel was a concern because randomizing of the steel properties through shuffling of laminations was not practicable in a job this large.

The yoke laminations were punched (fine blanked) from 6.35 mm thick ultra-low-carbon steel plate furnished by the Kawasaki Steel Corporation, Japan. Both the mechanical and magnetic characteristics of the steel are important in this application [18]. The yield strength of the steel was specified to be no less than 221 MPa, a level achieved through cold-rolling thickness reduction. This allowed the laminations to be pressed onto the coils without significant yielding on the mid-plane where the forces during collaring are high. To achieve control of the important high-field saturation magnetization (M_s), the chemical composition (impurities) was strictly specified. This control of the chemistry also ensured that important low field parameters like the coercivity H_c remained under control. Measurements on ring samples [19,20] and chemical analysis of extracted pieces of the production steel were used to monitor the quality of the steel, but the tight quality control exercised by the company in producing the steel ensured that all the material delivered was of the required accelerator quality.

The laminations have an inner diameter of 119.4 mm and an outer diameter of 266.7 mm. They were pinned together in pairs to allow the yoke elements to act as collars. To meet the rms tolerances for the magnetic field integrated over the length of the dipoles, it was required that the weight of steel in the yoke be controlled to within 0.07%. To achieve this tolerance, the lamination pairs that make up the yoke were weighed and their number adjusted to meet the weight specification. The selection of yoke pairs for the top and bottom halves was done in such a way that the total weight of the top half was slightly lower than that for the bottom half [21]. This helped to reduce the skew quadrupole at high fields resulting from a vertically off-centered cold mass in the cryostat (see Fig. 2). During magnet assembly, a press

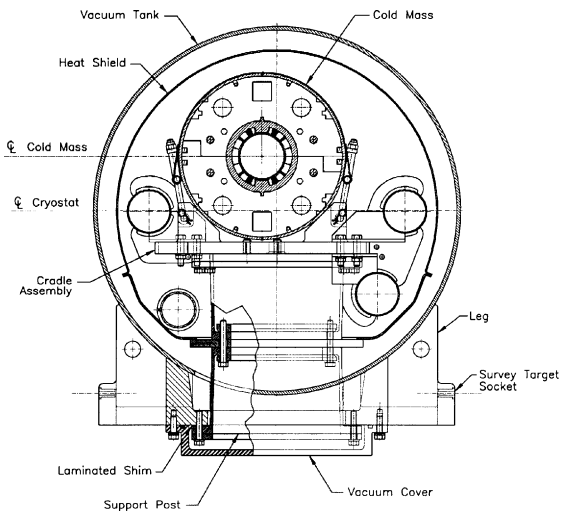

Fig. 2. A cross-section of the cryostatted dipole magnet. This section is at the magnet axial center, where the cold mass horizontal offset due to curvature is evident.

compressed the yoke around the coils. The yoke was subsequently held together with stainless steel keys pushed into notches on the outer circumference. The design preload of 70 MPa acting on the coils was routinely achieved. The yoke laminations extend the full length of the magnet and are not terminated prior to the coil ends as is done in many designs to reduce the field in the mechanically difficult end region of the coils.

3.5. Shell

After completion, the coil-in-yoke assembly was surrounded with two, 4.9 mm thick, type 304L stainless steel half-shells, which were then welded along the vertical mid-plane. The root pass of this weld joined the shell directly to the yoke laminations; no backing strip was used. Extensive testing at Brookhaven confirmed that the joining of these two dissimilar materials gave acceptable results. Nevertheless, a high-nickel-content filler material, type 385LN, was used in this and in the subsequent fill passes to increase the fracture toughness of the joint. In production, these welds were made by automated TIG machines.

Before the welding began, the magnet was placed in a fixture that introduced the required 48.5 mm sagitta; this sagitta was locked in place when the stainless steel half-shells were then welded together. The welding operation also formed the outer, high-pressure (2.1 MPa) helium containment vessel. The shrinkage of the weld compressed the steel collar block, ensuring closure of the mid-plane yoke gap. Further compression was realized at operating temperature from the differential contraction of the stainless steel shell relative to the steel yoke. Compression of the coil increased only until the yoke mid-plane gap closed.

3.6. Electrical connections and quench protection

The design of the machine uses separate main electrical bus systems for the dipoles and the quadrupoles. The bus conductor for these and the various corrector magnets was placed inside an insulating "pultrusion" that was then installed as a completed package into the bus slots at the top and bottom of the yoke. The electrical connections between bus conductors and magnet leads are at the ends of the magnets, within the volume defined by the stainless steel helium containment vessel and end can. The end volume also contains the Ω-type thermal expansion joints for the bus conductors and the quench protection diodes. Heaters consisting of small-diameter stainless steel pipe were installed to accelerate the occasional warm-up of the cold mass.

The quench protection diodes were constructed using a 76.2 mm diameter doped silicon element manufactured by Powerex Corporation, Youngwood, PA. The elements were from an existing compression style hockey puck product line with the diffusion process modified to achieve the cryogenic requirements. For the RHIC application, a non-hermetic assembly was required. The assembly includes two large copper masses as heat sinks and as compression contacts to the element, and a stainless shell with a threaded top cap. The surface contact with the element is a 76.2 mm circle, loaded to 53.4 kN contact force. The pressure loading is through two 19 mm diameter ceramic balls axially configured to assure an even, concentric loading of the diode element. The top cap is finally welded to the assembly body to prevent thread disengagement during the application of 7000 A test pulses, done at cryogenic temperature. Since the diodes are not hermetic, the polyimide passivation of the junction edge is of paramount importance, and required both visual and electrical screening to verify passivation integrity.

Early in the R&D project, measurements were made of $\int I^2\,\mathrm{d}t$ ($10^6\,\mathrm{A}^2\,\mathrm{s}$ or MIITS) versus temperature for a preliminary version of a RHIC dipole [22]. This enabled calibration of a model used for predicting the quench energy margins in the final version of the RHIC dipole. Estimates of worst case $I^2\mathrm{d}t$ values for conductor with the nominal parameters and a single quench protection diode for each magnet give a value of about 12.4 MIITS, compared with an estimated cable damage level of 13.8 MIITS. This converts to a temperature margin of about 250 K before the damage temperature of 835 K is reached. Thus, due to the extra copper in the superconducting strand, quench protection is achieved for the

Table 6
Electrical design parameters of the dipole magnet

Parameter	Value
Dipole bus stabilization copper (mm^2)	58
Bus expansion joint motion (mm)	46
Warm-up heater, resistance per heater at 300 K (Ω)	2.24
Warm-up heater, power per heater (W)	938
Quench protection diode, max. dissipation energy (kJ)	140
Quench protection diode, max. reverse leakage current at 1 kV (mA)	10
Quench protection diode, 4.2 K forward voltage threshold at 10 mA (V)	3

magnets with a single cold diode across the leads of each magnet, and no active quench protection circuitry. Some electrical design parameters for the dipole magnet are listed in Table 6.

3.7. Cryostat

The cryostated magnet is shown in Fig. 2. The major components are the carbon steel (ASTM A53) vacuum vessel (outer diameter 610 mm, wall thickness 6.4 mm), the aluminum heat shield (1100-H14) maintained at a nominal temperature of 55 K, blankets of multilayer aluminized Mylar thermal insulation, various cryogenic headers including bellows at their ends, and post-type supports [23] that carry the cold mass weight to the wall of the vacuum tank. Each support post is comprised of two identical molded plastic "hats" attached end to end. They were precision molded as tubes with flanges from Ultem 2100 glass-filled plastic. A standard arc dipole has three such supports. They make sliding contact (where necessary) to the cold mass to support the cold mass inside the cryostat. A spring was incorporated into this contact assembly to maintain the horizontal alignment of the cold mass. In the tunnel, only two stands carry the load to the ground. The weight distribution is 40% on the center post and 30% on each of the outer posts. The post inner diameter is 212.8 mm with a wall thickness of 4.8 mm. The heat shield is captured between the top and bottom hats. The heat leak per leg is 0.1 W to 4.5 K and 1.0 W to 55 K. The superinsulation blankets use alternating layers of reflectors (6 μm non-crinkled Mylar, aluminized on two sides) and spacers (0.15 mm REEMAY 2006). In order to minimize the heat load, the thickness of the aluminum on the Mylar used at 4.5 K is thicker (600 Å) than that on the Mylar at 55 K (380 Å) because of the difference in wavelength of the shielded radiation. The legs of the vacuum chamber are carbon steel castings welded to the vacuum vessel. Sockets machined into these legs are used to provide the exterior survey fiducial references; survey fixtures translate the positional information provided by the cold mass to these references.

3.8. Magnet manufacture, delivery and acceptance

A total of 373 dipole magnets was manufactured at Grumman according to prints and specifications developed by Brookhaven [24–26]. They were delivered as complete units ready for installation into the RHIC lattice. Superconducting cable, beam tubes and quench protection diodes were supplied by Brookhaven; all other components were procured by Grumman. During their construction, the magnets were subjected to rigorous quality and performance checks designed to prevent the manufacture of any faulty magnets. This goal was achieved; all magnets delivered to Brookhaven were acceptable for machine use. The initial 30 magnets were cold tested at Brookhaven. Upon confirmation that their performance validated their design and manufacture, only about 10% of the remaining magnets were cold tested. This reduced level of testing, and the resultant significant cost savings, has been proven sound by the subsequent stellar magnet performance in the machine. Warm magnetic measurements were made on all magnets, both at Grumman [27] and at Brookhaven, and the good warm–cold correlation has been used in tracking calculations at Brookhaven to predict machine performance.

3.9. Performance

Quench test results for the 51 arc dipoles tested at 4.5 K are shown in Fig. 3. The magnets were quenched until a "plateau," where there was little

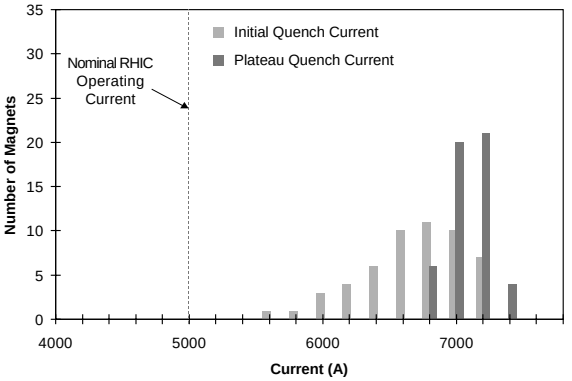

Fig. 3. Quench performance of 51 arc dipoles, tested at 4.5 K. The average plateau quench current of these 51 magnets was 7101 A; the field at this average quench current is 4.52 T.

variation in quench current, was reached, typically within a few quenches. The quench performance of the magnets was excellent. The initial quench current and the plateau quench current of each magnet exceeded the 5 kA operating current. The plateau quench currents were consistent with the currents expected for magnets operating at the current-carrying limit of the superconductor. In RHIC operations, the rings have reached 5 kA without quenching the arc dipoles, confirming the good construction of these magnets.

Magnetic measurements were made with two probes: a 1 m-long rotating coil with attached gravity sensor and a 10 m-long stationary coil. The 1 m coil was used to measure the harmonics and the field angle. Integral values of the harmonics and field angles at 4.5 K were obtained by moving the coil in ten 1 m steps at three currents: near injection (660 A), at transition in RHIC (1450 A), and at full energy (5 kA). Measurements were also made at closely spaced current steps with the coil at a fixed axial position near the center of each magnet. The 10 m stationary coil was used to measure the integral dipole field. The 1 m and the 10 m coils were also used for "warm" measurements with the magnets at room temperature.

During production, several changes were made to the magnet cross-section and, thus, to the geometric harmonics [28]. Planned changes were introduced in order to reduce the harmonics. Some unplanned changes in transfer function occurred due to variations in the materials used in the magnets. These changes were corrected before too many magnets were affected. The impact of affected magnets on RHIC was reduced by carefully assigning magnets with lower than normal transfer function to lattice locations next to magnets with higher than normal transfer function [29].

The field quality of the magnets at room temperature ("warm") was well correlated with the field quality at 5 kA ("cold"). Integral measurements of the low-order harmonics (normal and skew quadrupole, normal sextupole, and normal decapole) are shown in Figs. 4–7. (The

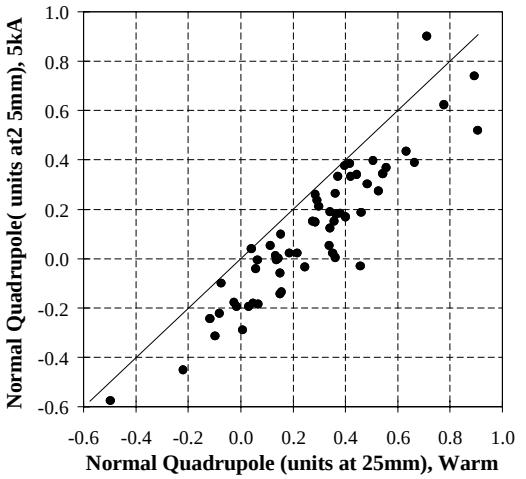

Fig. 4. Measured warm–cold normal quadrupole correlation.

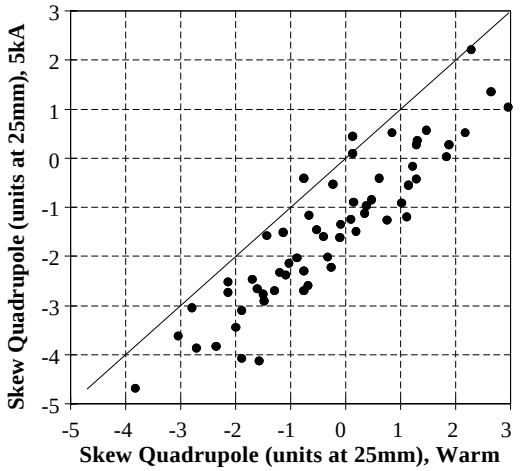

Fig. 5. Measured warm–cold skew quadrupole correlation.

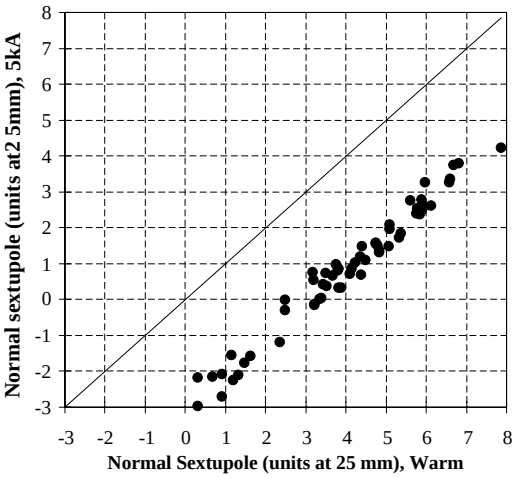

Fig. 6. Measured warm–cold sextupole correlation.

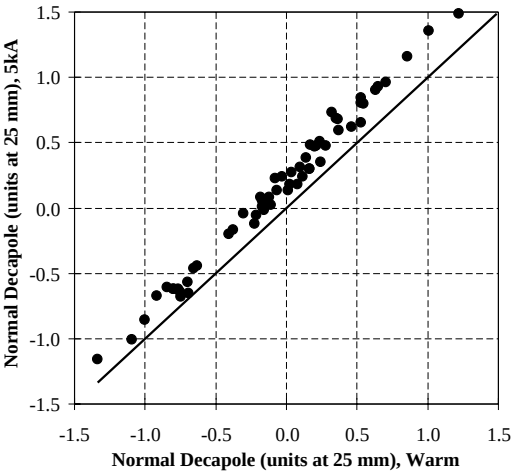

Fig. 7. Measured warm-cold decapole correlation.

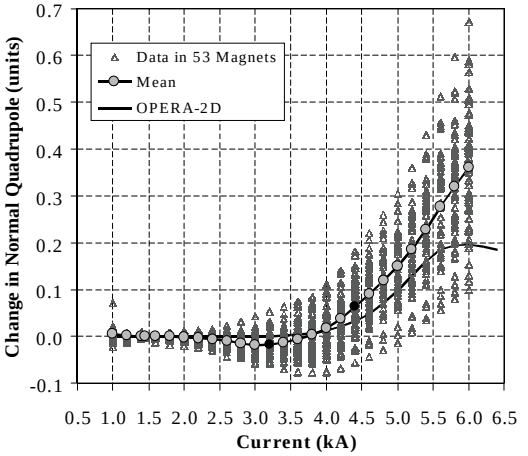

Fig. 8. Current dependence of the normal quadrupole component in the 80 mm dipole.

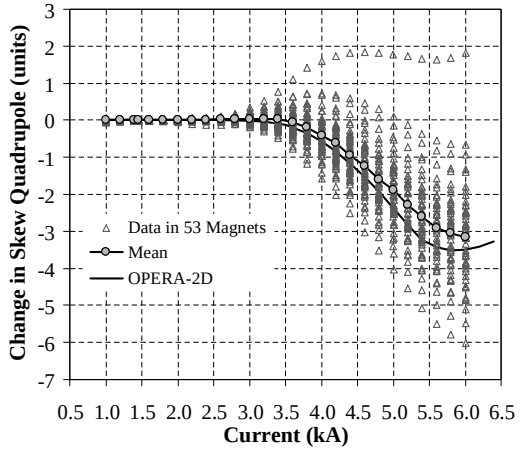

Fig. 9. Current dependence of the skew quadrupole component.

data do not lie on the straight line in the plots because of effects such as saturation.) Measurements of these same four harmonics as a function of current, in the straight section of the magnets, are shown in Figs. 8–11, along with the calculated values. Warm and cold measurements of the harmonics through the 22-pole term are given in Table 7. (Note that the quadrupole term is denoted by $n = 1$. Harmonics are expressed in "units", where a unit is 10^{-4} of the main field.)

The rms variation of the integral transfer function B/I measured warm in all the 9.7 m dipoles was 3.2×10^{-4}. The distribution of the ratio between the integral transfer functions measured warm and at 1.45 kA had an rms of 1.8×10^{-4}. A measurement of the transfer function in the straight section of the magnet whose transfer function is closest to the mean is shown in Fig. 12. The mean systematic twist of the dipoles was 0.6 mrad, with a rms of 2.2 mrad.

The time dependence of the 80 mm dipoles was determined from measurements in one of the 2.95 m-long magnets built for the D6 and D9 positions (see Table 1). The measurements were

focussed on the time dependence during injection and at the start of the ramp up [8]. The 1 m tangential measuring coil was located in the straight section of the magnet. Measurements were made with a time resolution of ~0.66 s. A smooth current ramp with a quadratic dependence of current on time was used. Prior to the measurement, the magnet was cycled from 25 A to 5.1 kA and back to 25 A at 60 A/s. The magnet was then ramped to 470 A at 40 A/s, held at that

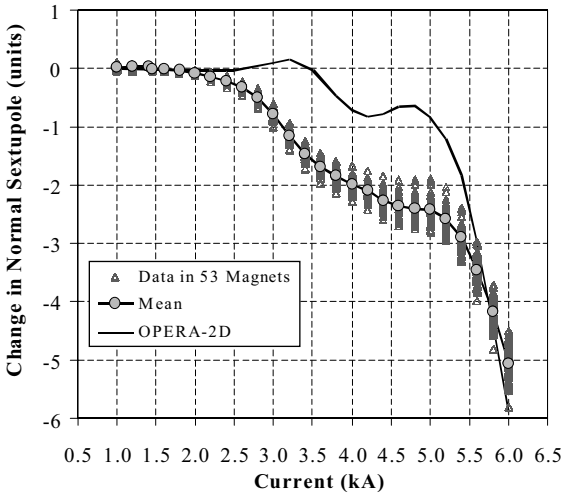

Fig. 10. Current dependence of the normal sextupole component.

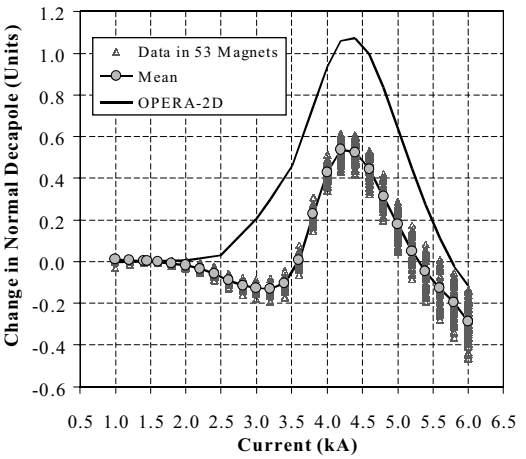

Fig. 11. Current dependence of the normal decapole component.

Table 7
Summary of the measured integral field harmonics in the 80 mm aperture, 9.7 m long dipoles. The 30 A measurements were done while the magnet was at room temperature. Harmonic b_1 is the normal quadrupole term

Harmonic	Mean			Standard deviation		
	30 A (296 magnets)	660 A (58 magnets)	5000 A (59 magnets)	30 A (296 magnets)	660 A (58 magnets)	5000 A (59 magnets)
b_1	0.25	0.08	0.10	0.37	0.28	0.28
b_2	3.54	−0.17	0.83	1.74	2.22	1.76
b_3	−0.03	0.00	0.01	0.10	0.08	0.08
b_4	0.22	-0.33	0.15	0.44	0.57	0.59
b_5	0.01	0.00	−0.03	0.03	0.03	0.04
b_6	0.12	−0.13	1.19	0.11	0.13	0.14
b_7	0.00	−0.01	−0.01	0.01	0.01	0.01
b_8	0.09	0.14	0.12	0.11	0.12	0.12
b_9	0.00	0.02	0.02	0.01	0.02	0.02
b_{10}	−0.53	−0.58	−0.58	0.02	0.02	0.02
a_1	−0.20	0.28	−1.51	1.62	1.53	1.51
a_2	−1.11	−1.03	−1.07	0.20	0.17	0.18
a_3	−0.01	−0.03	−0.36	0.49	0.42	0.41
a_4	0.18	0.21	0.20	0.07	0.06	0.06
a_5	−0.01	0.02	−0.06	0.17	0.15	0.16
a_6	−0.11	−0.10	−0.10	0.03	0.02	0.02
a_7	0.00	−0.01	−0.01	0.05	0.05	0.05
a_8	0.02	0.02	0.02	0.01	0.01	0.01
a_9	0.00	0.04	0.04	0.01	0.02	0.02
a_{10}	−0.01	−0.01	−0.01	0.00	0.01	0.01

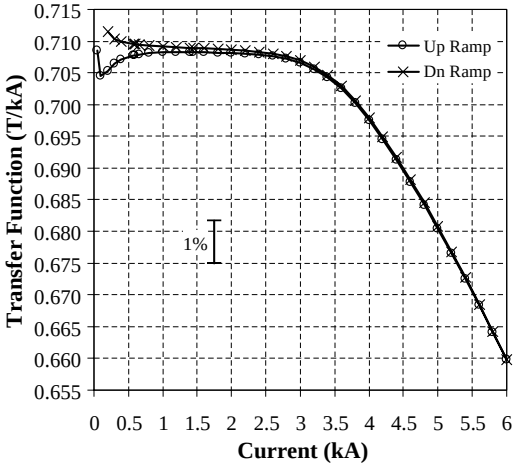

Fig. 12. Transfer function for a typical 80 mm dipole in the straight section.

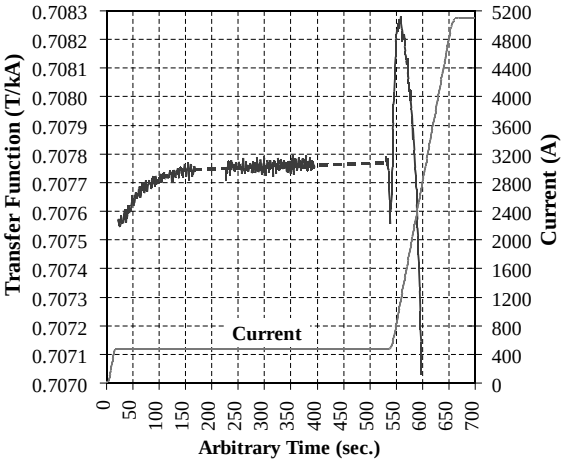

Fig. 13. Time decay and snapback in D96525.

current, and then ramped up at 40 A/s. The time variation of the transfer function and the current for injection and the initial part of the ramp up are shown in Fig. 13. The change of the transfer function at injection current and the "snapback" at the start of the ramp can be seen in the data. The drift and snapback of the sextupole were ~1.5 units. The snapback to the initial value occurs when the current has increased from 470 to ~498 A. The snapback is faster at higher ramp rates (~5–6 s at 20 A/s, ~2 s at 70 A/s). Because the superconductor was purchased as a single lot, it was expected that magnets of the same type would behave in a similar way. This was confirmed by measurements made on the RHIC beam [30].

4. Standard aperture quadrupoles

The standard aperture (80 mm) quadrupoles [31–33] share many of the design features of the standard aperture (80 mm) dipoles. Common features include superconducting cable, similar operating current, single layer coil, coil radius, yoke design, and beam tube. Several different lengths of these magnets were required, as listed in Table 1. The cold masses were built by the Northrop Grumman Corporation under a build-to-print contract. A cross-section of the magnet is shown in Fig. 14.

Each of the four coils in a quadrupole was wound with 16 turns of superconducting cable and a single, symmetric copper wedge to shape the field. After yoke assembly, the quadrupole cold mass was fitted with end plates that were held by tie rods extending through the magnet. These tie rods served to precisely fix the length of the magnet, and they resist the axial Lorentz force when the magnet is powered. This assembly was enclosed in stainless steel shells along with a corrector magnet at one end and a sextupole magnet at the other (called a "CQS" assembly).

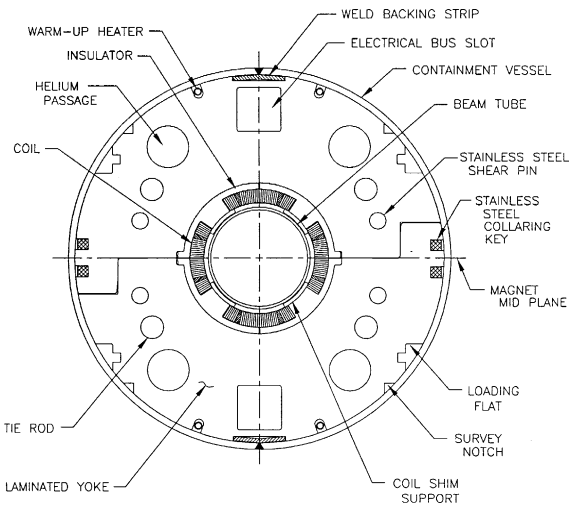

Fig. 14. Cross-section of the arc quadrupole magnet.

The shells were then welded, forming the support structure and a helium containment vessel. This construction step was done at Brookhaven on special tooling designed to maintain close positional tolerances of the cold masses. This basic CQS assembly was inserted into a cryostat and was then installed adjacent to every dipole in the RHIC arcs, forming the machine's lattice. Similar assemblies were also used in the insertion regions. Required gradients for the insertion region quadrupoles Q4, Q5, and Q6 are 6% higher than for the other quadrupoles of this design. The ample margin available in the design easily provides this higher field. As are the arc dipoles, these magnets in the machine are protected by a diode across the windings. Some quadrupole parameters are given in Table 8.

All quadrupoles quenched well above their operating current and most reached the conductor limit in a few quenches (Fig. 15). Measurements of the integral quadrupole field and the first allowed term are shown for a typical quadrupole in Figs. 16 and 17. Measurements of the transfer function during injection and the initial part of the ramp up are shown in Fig. 18 for a Q7 quadrupole. Measurement conditions were essentially identical to those for the dipole measurements discussed previously, except that the measuring coil was 0.23 m long. The drift and snapback of the dodecapole were ~1.5 units. Field quality data for the quadrupoles are summarized in Table 9.

Table 8
Selected parameters of the arc quadrupole magnet

Parameter	Value
Gradient at top energy (T/m)	71
Current at top energy (A)	4720
Gradient at quench (T/m)	107
Magnetic length (m)	1.11
Cold mass length (m)	1.305
Inductance (mH)	2
Stored energy (kJ)	20

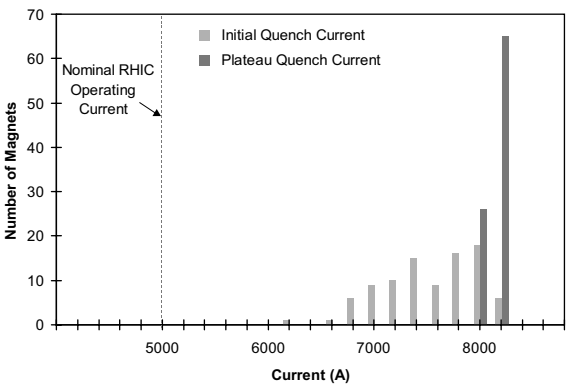

Fig. 15. Quench performance of 91 arc quadrupoles, tested at 4.5 K. The average plateau quench current of these 91 magnets was 8152 A.

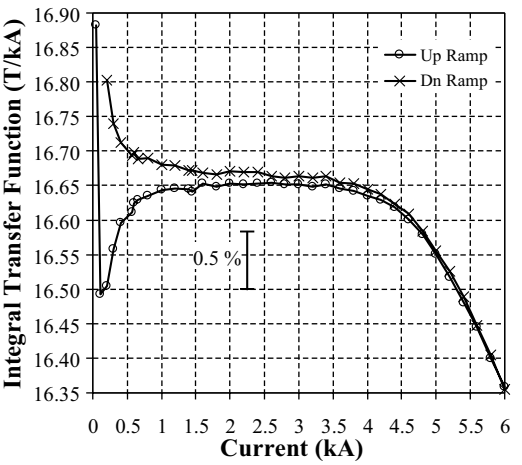

Fig. 16. Integral transfer function in QRG316.

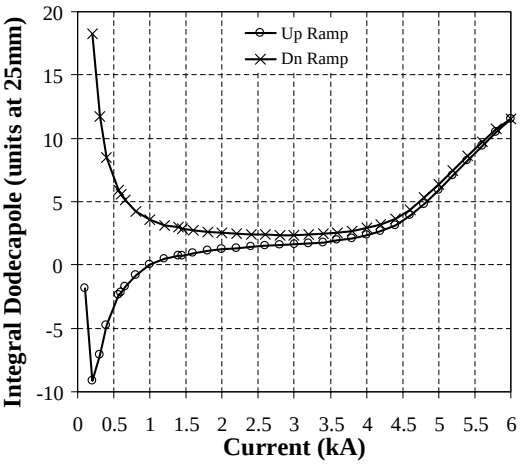

Fig. 17. Integral dodecapole in QRG316.

5. Sextupoles and trim quadrupoles

Sextupole magnets in RHIC [34] compensate for the natural chromaticity of the machine and correct for the sextupole field generated in the dipoles by iron saturation and superconductor magnetization. They are located at each arc quadrupole and at the Q9 quadrupoles in the 3–4, 7–8 and 11–12 o'clock insertions. Because of the required field strength, they were built as separate, dedicated magnets rather than as part of a correction package. The sextupole cold mass cross-section is shown in Fig. 19. These were manufactured by Everson Electric Corporation, Bethlehem, PA.

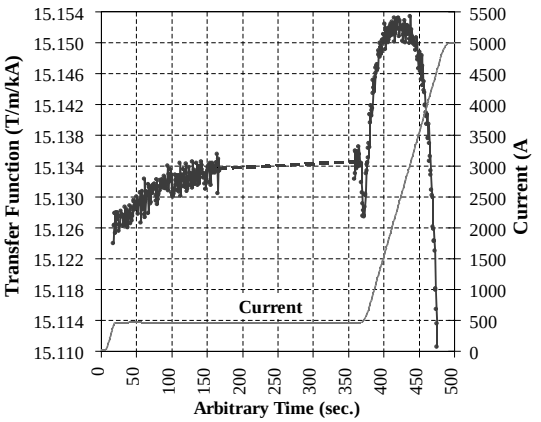

Fig. 18. Time decay and snapback in QR7109.

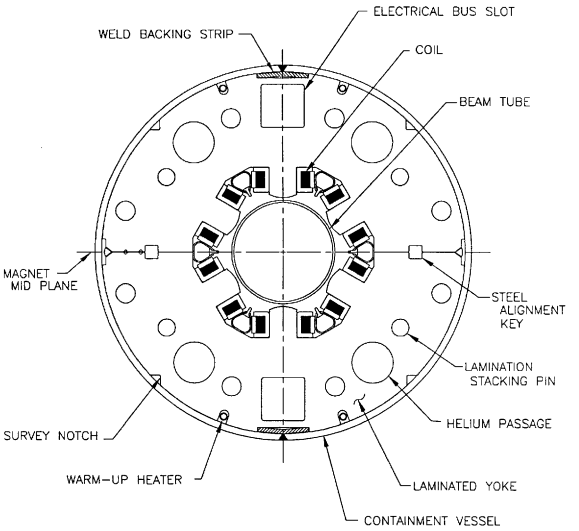

Fig. 19. Cross-section of the sextupole magnet. The coils are held in place by beryllium copper retainer springs and aluminum locking wedges (not labeled).

Table 9
Summary of integral field quality in RHIC arc quadrupoles

Harmonic at 25 mm	Mean		Standard deviation	
	10 A (380 magnets)	5000 A (91 magnets)	10 A (380 magnets)	5000 A (91 magnets)
b_2	−0.61	−0.21	1.61	1.77
b_3	−1.51	−0.61	0.95	1.39
b_4	0.14	0.57	0.49	1.57
b_5	1.42	5.70	0.42	0.62
b_6	0.01	0.05	0.13	0.13
b_7	−0.52	−0.52	0.09	0.11
b_8	0.01	0.06	0.05	0.14
b_9	−1.29	−1.44	0.06	0.08
b_{10}	0.00	0.00	0.02	0.02
a_2	−1.93	−1.83	1.66	1.68
a_3	0.48	0.23	0.95	0.90
a_4	0.06	−0.26	0.48	1.40
a_5	−3.76	−3.84	0.29	0.31
a_6	0.04	0.06	0.13	0.14
a_7	0.01	0.04	0.11	0.09
a_8	0.00	0.03	0.05	0.10
a_9	0.35	0.39	0.02	0.04
a_{10}	0.00	0.00	0.02	0.02

The field shape is dominated by the iron yoke, easing the construction tolerances for the six coils in each magnet. These are wound from NbTi multifilamentary wire, listed in Table 4. They consist of 200 turns of wire, wrapped with 25 μm Kapton insulation with 48% overlay and embedded in a fiberglass/epoxy matrix. They were machine-wound onto a machined G-10 form and secured to the pole tips of the yoke laminations, which were punched from 1.5 mm thick, low carbon steel sheet. A scheme employing beryllium copper retainer springs and aluminum locking wedges with intervening G10 insulator strips was used to secure the coils (Fig. 19). The sextupole cold mass surrounds a cold stainless steel beam tube of standard aperture common to the CQS assembly. The beam tube was welded at one end to a beam position monitor assembly which, in turn, was fastened to the stainless steel end plate of the sextupole yoke; thus, everywhere within the sextupole bore, the beam tube fits loosely within the confines of the pole tips. Some parameters of the sextupole magnets are given in Table 10.

The quench performance of sextupoles built as prescribed was excellent, with the magnets usually reaching the limit of the conductor in a few quenches, in both polarities. However, the quench performance of about 30 magnets was poorer, although adequate for operation at currents below 50 A. The cause of the problem was traced to an unauthorized change in production procedures. Fortunately, places were found in the lattice where the operating current was not expected to exceed 50 A. Thus far, no sextupole has quenched in RHIC.

The integral transfer function for a typical sextupole is shown in Fig. 20. The saturation of the pole tip is responsible for the decrease of the transfer function at high current and is in agreement with calculation. The large value (~1%) of the first allowed harmonic (Fig. 21) is a consequence of the simplicity of the coil construction and is acceptable for these magnets.

Table 10
Selected parameters of the sextupole magnet

Parameter	Value
Field at 100 A, 25 mm radius (T)	0.480
Maximum operating current (A)	100
Quench current (A)	200
Magnetic length (m)	0.75
Cold mass length (m)	0.82
Inductance at 100 A (mH)	530
Stored energy at 100 A (kJ)	2.64

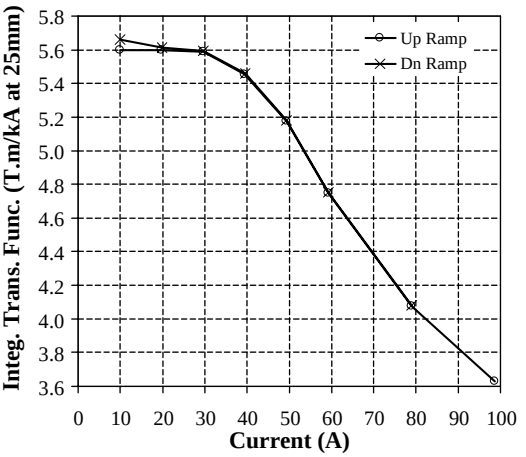

Fig. 20. Integral transfer function in SRE211.

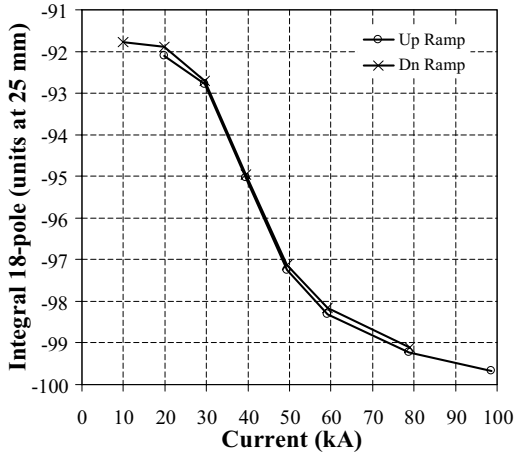

Fig. 21. Integral of the first allowed harmonic (b_8) in SRE211.

The space normally occupied by sextupoles in CQS assemblies at locations Q4, Q5 and Q6 was used instead for individually powered trim quadrupoles. The construction of these trim quadrupole cold masses [34] was substantially the same as that of the sextupole cold masses. A drawing of the

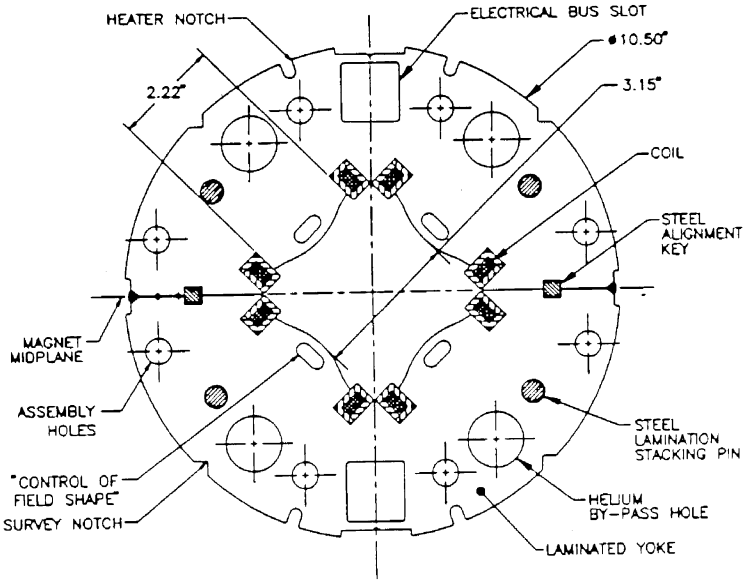

Fig. 22. Cross-section of the trim quadrupole magnet.

Table 11
Selected parameters of the trim quadrupole magnet

Parameter	Value
Gradient at 100 A (T/m)	29.4
Quench current (A)	182
Magnetic length (m)	0.75
Yoke length (m)	0.81
Inductance at 100 A (mH)	590
Stored energy at 100 A (kJ)	3

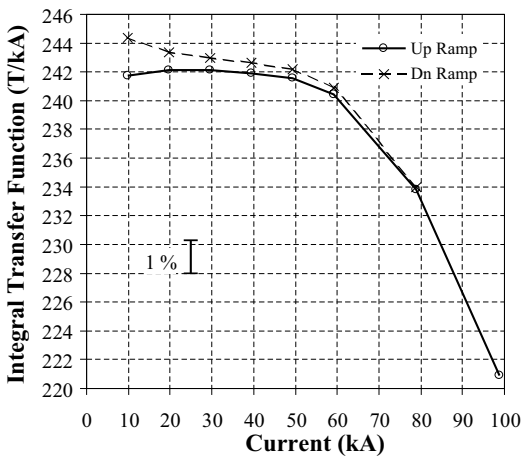

Fig. 23. Integral transfer function in trim quadrupole QRT148.

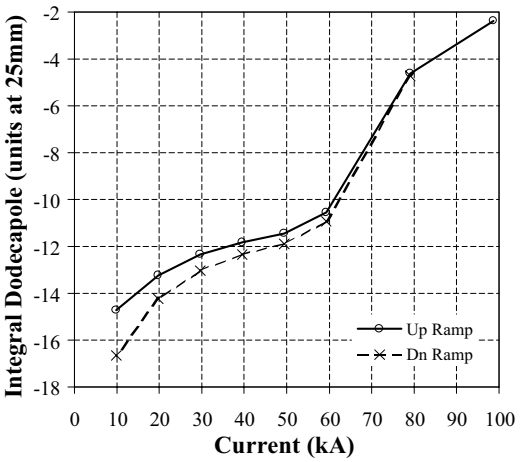

Fig. 24. Integral of the first allowed harmonic (b_5) in trim quadrupole QRT148.

cold mass cross-section is shown in Fig. 22 and a list of selected parameters is given in Table 11.

The quench performance of the trim quadrupoles was excellent, with the magnets reaching the conductor limit in a few quenches. The transfer function (Fig. 23) and first allowed harmonic (Fig. 24), plotted for a typical magnet, show a saturation behavior similar to but smaller than that of the sextupole.

Table 12
Selected parameters of the 80 mm corrector magnet

Style	Number	Position	Multipoles (b_1 = quadrupole, etc.)
B	96	Focusing quad	b_0, b_1, b_3, b_4
C	132	Defocusing quad	a_0, a_1, b_3, b_4
D	78	Focusing quad	b_0
E	78	Defocusing quad	a_0
F	36	Focusing quad	b_0, a_1, b_3, b_4

6. Standard aperture arc correctors

Corrector magnets are required throughout the machine to compensate for systematic and random errors of the magnets and to control various beam dynamic properties. The RHIC 80 mm correctors are nominally 0.5 m in effective length and are an integral part of the CQS package. They contain either four multipole elements or a lone dipole element, as shown in Table 12. Their design is novel and their manufacture (at Brookhaven) was largely automated [35,36].

The dipole correctors (b_0, a_0) correct the closed orbit error resulting primarily from random dipole rotational errors and quadrupole misalignments around the ring, necessitating individual current control in each corrector. For this reason, a design using relatively low current was adopted, reducing the size of the electrical bus work, power supplies and heat leaks in cryogenic current leads. The skew quadrupole correctors (a_1) correct the effect of random skew quadrupole errors in the main dipoles and random installation errors in the main quadrupoles. The decapole correctors (b_4) compensate for dipole iron saturation effects. The octupole correctors (b_3) are used for the correction of second order chromaticity effects. The octupole and decapole correctors have not been equipped with power supplies in the initial operation of the machine.

Fig. 25 shows a cross-section of the four-element arc corrector magnet cold mass and Fig. 26 shows the cross-section in greater detail. In radially increasing order, the coil structures are decapole, octupole, quadrupole, and dipole coils, respectively. Each of the inner three structures consists of a double layer of racetrack coils wound with a single, multifilamentary NbTi superconducting wire (see Table 4). The outermost winding, the

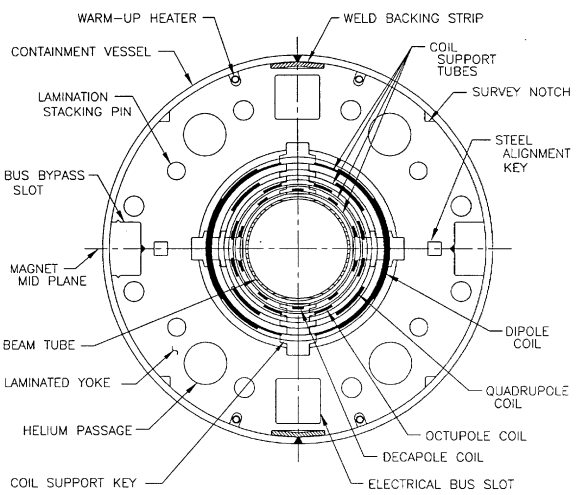

Fig. 25. Cross-section of the 80 mm corrector magnet.

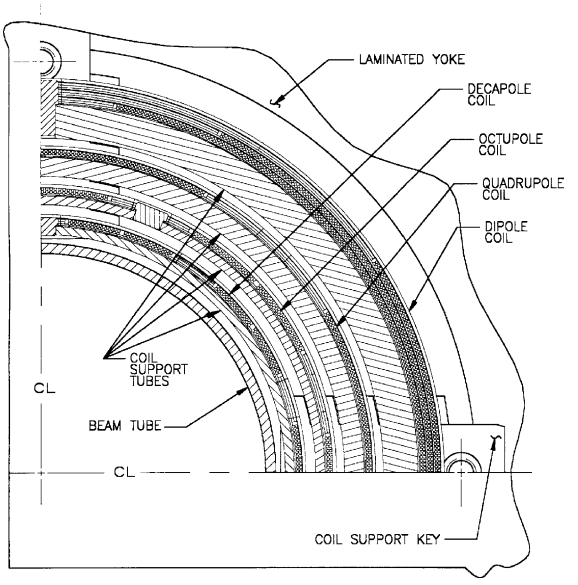

Fig. 26. A section of the 80 mm corrector magnet showing the coil layout in greater detail.

dipole, has three double layers of superconducting wire arranged to minimize field harmonics. Each double layer was machine-wound on a flat, flexible Kapton substrate. Subsequently, the substrate was epoxy-bonded to a stainless steel support tube that had previously been wrapped with Kapton and fitted with aluminum locating pins. A tensioned wrap of Kevlar cord, wetted with epoxy, was added to compress the package.

The physical length of the various corrector coils is nominally 0.58 m, a length short enough that the stainless steel support tubes can be supported solely at their ends. The tube diameters were selected from commercially available standard sizes to minimize machining. The dipole and quadrupole support tube thicknesses were chosen to make acceptable the distortions due to the predicted magnetic forces, and the octupole and decapole support tube thicknesses were determined by machining requirements. The end support is provided by separators, four at each end, which serve to position the tubes radially, azimuthally, and axially, and which tie into the overall CQS support and alignment structures. The yoke laminations are stamped from 1.5 mm thick low-carbon steel sheet. They have the same external configuration as the quadrupole and sextupole laminations. Assembly and alignment were as described for the arc quadrupole. A summary of the standard aperture corrector mechanical coil parameters required for each multipole is given in Table 13. Table 14 gives the operating parameters of the corrector magnets. In general, all the correctors are designed to operate conservatively at ~25–33% of their quench limit.

Table 13
Mechanical parameters of the 80 mm correctors coils. All coils are double layers

Multipole	Support tube o.d. (mm)	Turns/pole	Overall length (m)	Wire length (m)
Decapole	82.1	28	0.584	306
Octupole	92.0	38	0.583	359
Quadrupole	104.8	90	0.585	426
Dipole/1	122.5	278	0.580	660
Dipole/2		226		544
Dipole/3		122		307

Table 14
Operating parameters of the 80 mm correctors

Multipole	Inductance (mH)	I_{op} (A)	B at 25 mm (T)	L_{eff} (m)	I_Q (A)
Decapole	5.0	59.0	0.016	0.575	202
Octupole	8.0	50.6	0.017	0.571	198
Quadrupole	29.0	49.8	0.068	0.555	190
Dipole	840	52.2	0.577	0.508	160

Table 15
Integral field quality measured in the 80 mm corrector coils

Layer type	Transfer function, T m/kA at 25 mm (warm)	Std. deviation in TF (%)	Change in TF on cooldown (%)	Harmonics as fraction of the fundamental field (%)
b_0/a_0	5.5549	0.16	+1.0	<0.3
b_1	0.7627	0.18	+0.7	<0.6
a_1	0.7570	0.09	+0.7	<0.6
b_3	0.1920	0.53	+0.9	<2
b_4	0.1494	0.48	+1.2	<2

All correctors were quench tested because the conductor consists of a single strand, increasing the consequences of damage to a strand at any stage of production. In particular, careful study indicated that it would be difficult to detect damage during the automated coil winding process. Therefore, all corrector layers except for the dipole were tested to ±100 A, twice the maximum operating current. Dipoles were tested to ±70 A, since quenches at higher current could damage the magnet. Correctors other than the dipole were tested in self-field and in the background field of the dipole at 70 A. In all, 1229 layers were tested [37]. About $\frac{2}{3}$ of the layers reached the maximum current without quenching. Seven layers failed during quench test and were replaced.

The correlation between warm and cold field quality measurements was good enough that only ~20% were measured cold. The data for all the 80 mm correctors are summarized in Table 15. The reproducibility of the integral transfer function is typically 0.2%, and the harmonics are at the level expected for a corrector, ~1% of the fundamental. The standard deviation of the warm–cold difference in the integral transfer functions is less than 0.1% of the transfer function for the dipole and quadrupole coils and ~0.3% for the octupole and decapole coils.

7. Standard aperture CQS assemblies

The CQS assemblies consist of various combinations (over 80 types) of quadrupole, sextupole and corrector elements assembled together into a

common cold mass containment and vacuum vessel [38]. The weight of a CQS assembly is typically 948 kg. The quadrupole and sextupole elements were manufactured industrially, the corrector elements were manufactured in-house at Brookhaven. These elements, along with numerous other components, make up the single complete unit for the RHIC ring. Components included are recoolers for the main helium distribution circuit, beam position monitors, power leads for the included corrector magnets [39], and instrumentation and heater leads with the leads exiting the cryostat locally. Special tooling to control the positions and rotations of the elements during assembly, and instrumentation to measure these parameters afterwards [40–42], was developed. A special shell-welding technique was developed to remove any excessive residual twist in these assemblies as well as in the larger 130 mm assemblies [43]. Because of their ubiquitous location around the machine, a rigorous analysis of bellows' strength and operational range was performed [44,45]. This analysis describes the bellows required for interconnecting these devices to their neighbors in the rings. Fig. 27 shows the magnets of a CQS unit on the assembly bench.

The magnetic centers of the CQS elements were measured by two unusual methods: colloidal cell and harmonic antenna. A number of quadrupoles were measured by shining polarized light through a cylindrical glass cell containing a colloidal suspension of iron filings [41]. In a sufficiently strong field, the iron filings lined up along field lines enough to rotate the plane of polarization of the light. The light was viewed through a second filter, which was rotated 90° with respect to the first. The transmitted light produced field patterns that were accurate to $\pm 50\,\mu m$. Because of limitations in this technique, a more versatile device, the harmonic antenna, was developed. With this device, the field center was measured on all three elements of the CQS. The harmonic antenna is a stationary coil, 23 cm long, that senses the fields produced by AC currents in the range 10–20 Hz. The coil also has crossed wires mounted precisely across its ends, allowing its position to be surveyed relative to external fiducials to within 0.025 mm. The field center relative to the coil is also determined within 0.025 mm, even in measurements at room temperature [42].

The installation procedure for the CQS called for the centers of the quadrupole and sextupole to be installed on the central beam orbit, so the measurements were analyzed to report the "corrector offset," the distance between the center of the corrector and the beam orbit. After a learning curve, rms corrector offsets of 0.5 mm were achieved [46].

To establish the warm–cold correlations, the first 30 CQS units plus 18 of the remaining units were cold tested. For CQS units, the main focus of the correlation is the field angles. For both the quadrupole and the sextupole, the mean warm–cold difference in field angles was −0.2 mrad, with

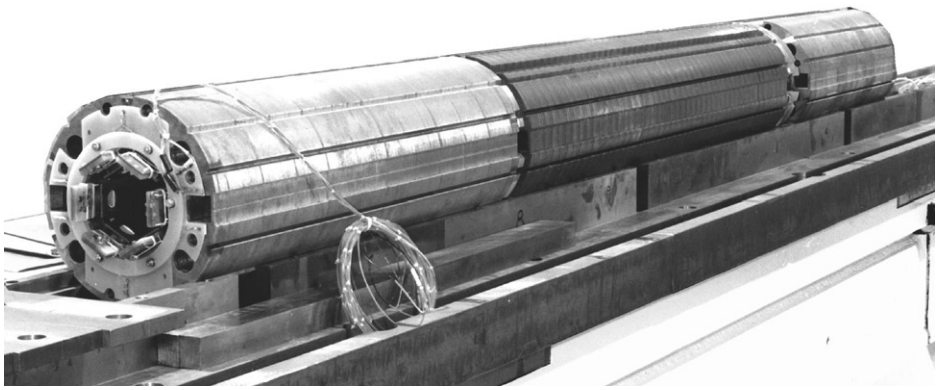

Fig. 27. The magnets of a CQS unit on the assembly bench. In the foreground is a sextupole cold mass, followed by quadrupole and corrector cold masses.

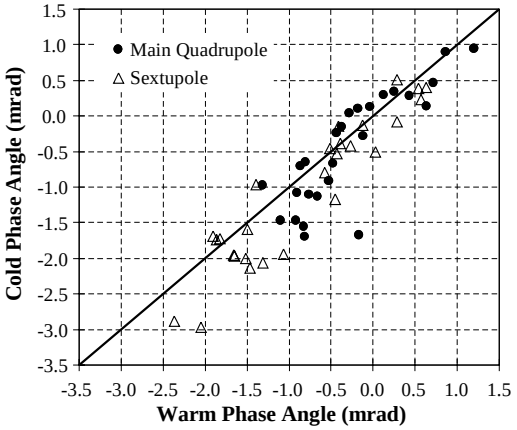

Fig. 28. Warm–cold correlations of CQS field angles.

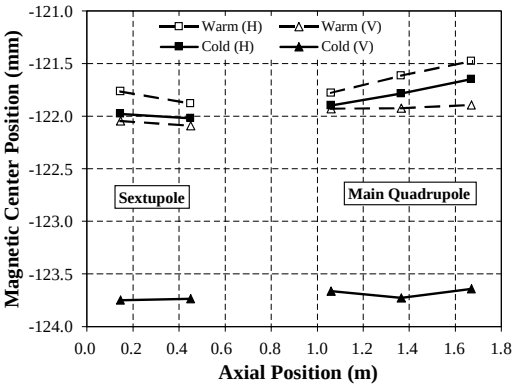

Fig. 29. Correlation between warm and cold centers in a CQS assembly.

an rms of 0.4 mrad (Fig. 28). For dipole correctors, the mean field angle difference was −0.3 mrad with an rms of 0.5 mrad. The centers of the magnetic field were measured warm and cold in one CQS (Fig. 29). The field center was measured at three axial positions in the quadrupole and two in the sextupole. The change in vertical position, about 1.75 mm, agrees with the change expected due to thermal contraction. The change in horizontal position is about 0.25 mm.

8. Large aperture insertion correctors

The large aperture triplet of quadrupoles Q1, Q2 and Q3 on each side of each crossover have associated 130 mm correctors [47], as listed in Table 16.

Table 16
Selected parameters of the 130 mm corrector magnets

Style	Name	Number	Position	Multipoles (b_0 = normal dipole, etc.)
I	C1	12	Outer ring, crossover end of Q2	b_0, b_3, b_4, b_5
J	C1	12	Inner ring, crossover end of Q2	a_0, b_3, b_4, b_5
K	C2	24	Inner/outer ring, crossover end of Q3	a_1, a_3, a_2, a_5
L	C3	12	Inner ring, non-crossover end of Q3	b_0, b_3, b_2, b_5
M	C3	12	Outer ring, non-crossover end of Q3	a_0, b_3, b_2, b_5

The correctors coils were made in the same way as those for the arc correctors, using the same type of double-layer coils. Their nominal magnetic length is 0.5 m and each element has a nominal operating current of 50 A. The iron lamination inner diameter is 200 mm and the outer diameter is 350 mm. The assembly that holds the coils in the yoke was similar to that of the arc corrector, but with the added provision to individually shim each corrector element to the required horizontal and vertical position inside the yoke. Table 17 shows the winding packages for each corrector element and other salient parameters.

All of the correctors were quench-tested using the same protocol as for the 80 mm correctors. Three coils out of a total of 315 needed to be replaced. Nearly all of the remaining coils reached the test limit of 100 A (70 A for dipoles) without quenching.

The correctors were shimmed based on warm measurements and warm measured a second time to confirm the effect of the shims. The shimming significantly reduced both the field angle and the off-axis distances of the individual layers. The field angles were adjusted to be within ± 1 mrad of nominal. The alignment relative to the center of the yoke was within ± 0.2 mm. A summary of the field quality measurements is given in Table 18.

Table 17
Additional parameters of the 130 mm corrector magnets

Parameter	a_0/b_0	a_1	a_2/b_2	a_3/b_3	b_4	a_5/b_5
Layers	6	2	2	2	2	2
R outer (mm)	97	95	76	82	76	69
R inner (mm)	93	93	73.5	80	73.5	67
Turns/pole/layer	149	79	41	33	23	17
Field at 40 mm, 50 A (T)	0.570	89.2×10^{-3}	41.2×10^{-3}	17.3×10^{-3}	10.4×10^{-3}	8.24×10^{-3}
L (mH)	1710	112	30	26	14	8.6

Table 18
Summary of field quality measured at room temperature in all the 130 mm corrector coils

Coil type	Integral transfer function (T m/kA at 40 mm)	Standard deviation of integral transfer function (%)	Harmonics at 40 mm radius (%)
Dipole	5.572	0.15	<0.3
Quadrupole	0.8792	0.09	<0.3
Sextupole	0.4023	0.12	<0.7
Normal Octupole	0.1686	0.17	<1.0
Skew Octupole	0.1678	0.17	<0.7
Decapole	0.1017	0.15	<1.2
Dodecapole	0.0798	0.45	<1.0

9. Large aperture insertion quadrupoles

Large aperture (130 mm) quadrupoles [48] are located on each side of the crossing points, arranged in a triplet configuration. They focus the beams to a minimum size at the crossing point. Because the beam size is large in these magnets, good magnetic field quality was an important goal in the design. The inner and outer beams each traverses an independent set of these quadrupoles; the beams do not share a common aperture. Their mechanical construction is similar to that of the standard aperture quadrupoles: single layer coils but made with a 36-strand cable, phenolic spacers, and a yoke acting as a collar to prestress the coils. A cross-section drawing of the cold mass is shown in Fig. 30.

Each of the four coils in a quadrupole was wound with 27 turns of cable and two copper wedges for field quality control. The iron yoke was designed to maintain quadrupole symmetry so far as possible, while also allowing for the necessary

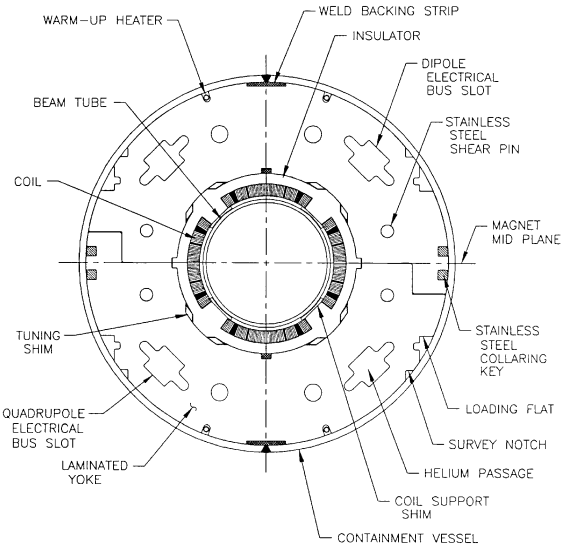

Fig. 30. Cross-section of the 130 mm quadrupole magnet.

bus work, helium circulation, mechanical features, and saturation control. The yokes are enclosed in a stainless steel shell, along with corrector magnets, to give mechanical rigidity and helium containment. The technique of applying weld stripes to the shell to reduce twist, first used on the arc dipoles, was applied here as well. The rms twist on the Q2's was reduced from 1–2 mrad to less than 0.5 mrad [43]. These cold masses as well as those in the neighboring ring and the adjoining D0 bending magnets were all built into a common vacuum tank in situ. Some basic parameters are given in Table 19.

Several design modifications were made to improve field quality after two magnets had been built. Measurements revealed that quadrupole symmetry had not been completely realized during

construction. To compensate, the coil-to-coil gaps at 0° and 180° were increased to 0.25 mm and those at 90° and 270° to 0.15 mm. Measurements also showed substantial harmonics, both normal and skew, in the lead end due to placement of the eight leads as they exit the coil proper. It was found that this could be ameliorated by rotating all eight leads (which alternate in current direction) 90° azimuthally in the magnet end space in such a way that roughly equal lengths of lead, with opposing current direction, occupy each azimuthal position. The integrated harmonics in this space were thereby reduced or eliminated.

To improve field quality still further, a new method was developed that allowed adjustment of the harmonics after the cold mass had been built [49]. Tuning shims were placed at the inner surface of the iron of each quadrupole after magnetic measurements had been made at room temperature. The tuning shim package was made up of a number of steel (magnetic) and brass (non-magnetic) laminations with a total thickness of 6.35 mm. These were inserted into the eight spaces symmetrically located between the phenolic spacers and the iron yoke. The packages were adjusted to reduce the measured values of the normal and skew sextupole, octupole, decapole, and dodecapole harmonics, based on the room temperature measurements.

Table 19
Selected parameters of the 130 mm quadrupole magnets

Parameter		Value
Gradient (T/m)	at top energy	48.1
Current (A)	at top energy	5050
Magnetic length (m)	Q1, Q2, Q3	1.44, 3.40, 2.10
Beam tube outer diameter (mm)		121
Iron outer diameter (mm)		350.5
Inductance (mH)	Q2	13
Stored energy (kJ)	Q2 at top energy	165

Results for the quench tests of the insertion quadrupoles are shown in Fig. 31. The first quenches of all but two of the magnets were above the 5 kA operating current. Later test protocol limited ramping to 7 kA. Quench origins were studied with both voltage taps and a quench antenna [50], but no single location was identified as limiting the performance. Additional quench testing was performed to verify that the magnets did not retrain after a thermal cycle. All of the Q1's and Q2's were cold tested, but only 13 of the Q3's. None of the insertion quads has quenched in RHIC.

Plots of the transfer function and first allowed harmonic versus current are given for a Q1 (Figs. 32 and 33), a Q2 (Figs. 34 and 35), and a Q3 (Figs. 36 and 37). The magnets shown are those closest to the mean for that length.

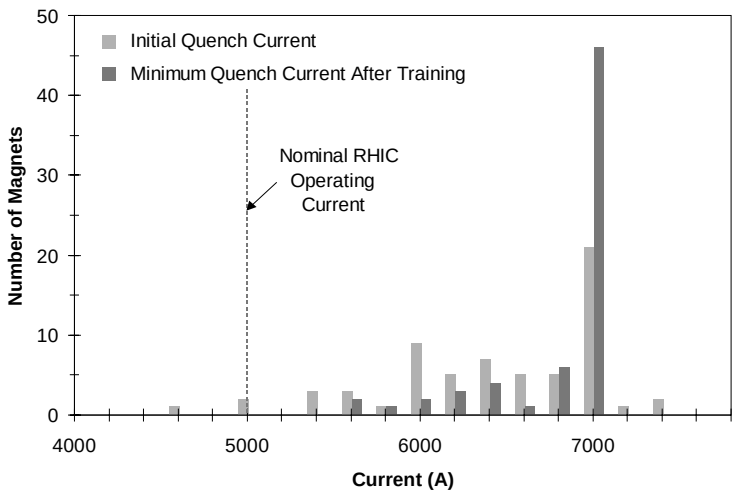

Fig. 31. Quench performance of 61 large aperture (130 mm) quadrupoles, tested at 4.5 K.

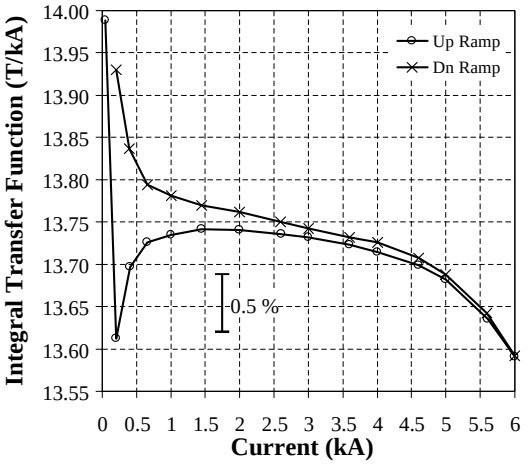

Fig. 32. Integral transfer function in Q1 magnet QRI114 (close to mean at 5 kA).

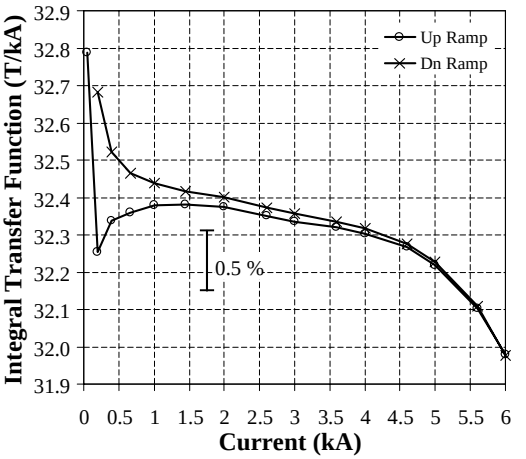

Fig. 34. Integral transfer function in Q2 magnet QRK119 (close to mean at 5 kA).

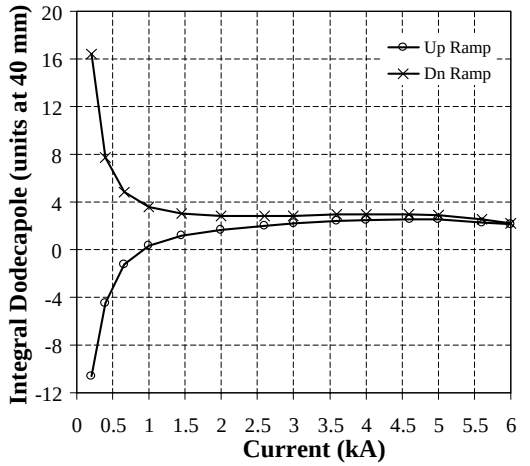

Fig. 33. Integral first allowed harmonic (b_5) in Q1 magnet QRI114.

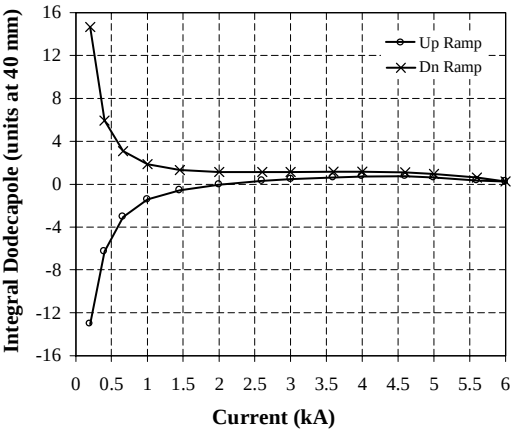

Fig. 35. Integral first allowed harmonic (b_5) in Q2 magnet QRK119.

Tuning shims were used to optimize the field quality at 5 kA, where the quadrupoles play the greatest role in beam performance. The use of tuning shims significantly improved the field quality of the quadrupoles, particularly for the low order terms (Fig. 38) [51]. There were several practical limitations to improving the field quality with the tuning shims. One is the uncertainty in the correlation between warm and 5 kA measurements. Saturation reduces the correlation with measurements made at lower currents. Figs. 39 and 40 show this effect for the normal sextupole. Also, warm–cold correlations must be established for each length of quadrupole, significantly lengthening the cold test time needed for the first magnets of each type. Another limitation is the change in harmonics with quenching or thermal cycle. Magnetic measurements were made before and after quench and thermal cycles on eight of the Q1's that were thermally cycled [52]. The rms of the change in the low-order harmonics due to quenching and thermal cycling was several tenths of a unit, somewhat smaller than the uncertainty in the warm–cold correlation.

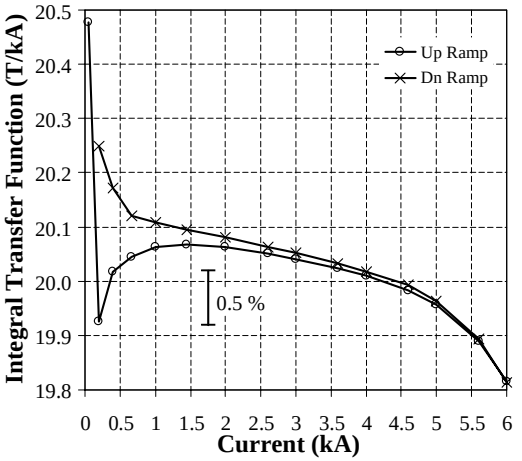

Fig. 36. Integral transfer function in Q3 magnet QRJ116 (close to mean at 5 kA).

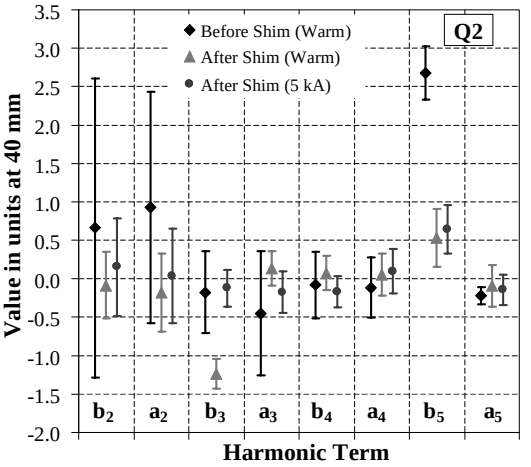

Fig. 38. Harmonics before and after shimming in the Q2 quads (QRK).

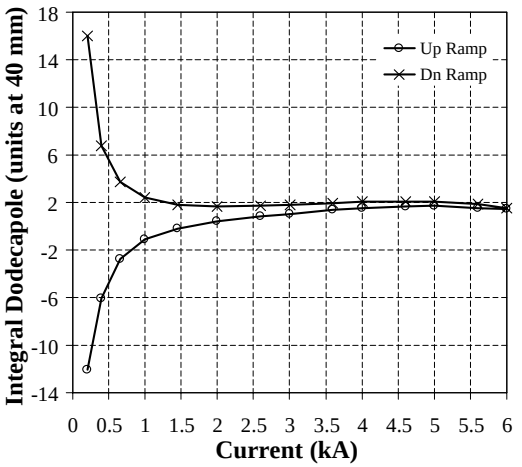

Fig. 37. Integral first allowed harmonic (b_5) in Q3 magnet QRJ116.

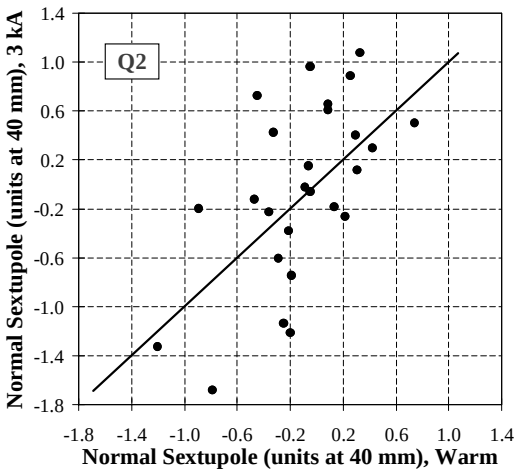

Fig. 39. Warm–cold correlation of b_2 in the Q2 (QRK) magnets at 3 kA.

The difference in the field quality requirements for the two "golden" IR's ($\beta^* = 1$ m) and the other four "non-golden" regions ($\beta^* = 10$ m) made it possible to use all of the quadrupoles built in RHIC [53]. Nearly all of the quadrupoles met the field requirements for "golden" IR's. The integral field quality data at 5 kA for all the magnets tested cold are given in Table 20. In early magnets of the Q1 and Q3 series, the first allowed harmonic, b_5, was larger than in later magnets.

10. Large aperture CQ assemblies

For these assemblies, the cold mass helium containment half-shells were welded around the individual quadrupoles and correctors. This was in contrast to the standard aperture CQS assemblies described earlier, where the half-shells were welded around the corrector, quadrupole, and sextupole cold masses as a single unit. There, the shortness of the quadrupoles allowed the use of internal tie

rods to support the quadrupole end plates, which restrain the axial Lorentz force of the coils. The greater length of these quadrupoles required the stiffness of the shell to act as support for the magnet end plates. Once fitted with its shell, each Q2 and Q3 quadrupole was welded end-to-end to its respective corrector or correctors to form a single CQ cold mass (Q2's had one corrector, Q3's had two). Weld stripes on the shell were used to improve the alignment of the correctors with respect to the quadrupoles [43]. For the CQ2 units, the mean corrector offset was 0.15 mm with 0.2 mm rms. For the CQ3 units, produced later, the mean was 0.04 mm, with 0.16 mm rms. Nearly all the correctors had offsets less than 0.5 mm. CQ assemblies were not cold tested.

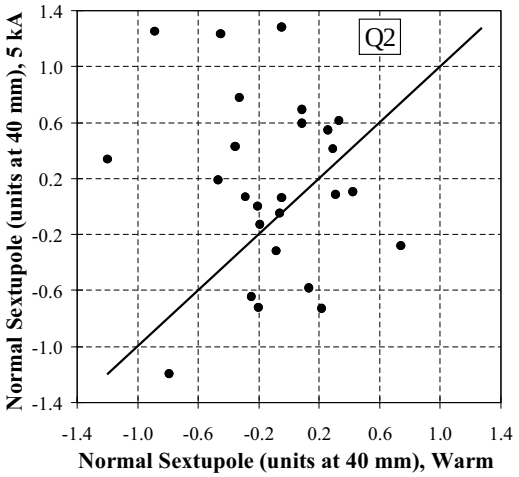

Fig. 40. Warm–cold correlation of b_2 in the Q2 (QRK) magnets at 5 kA (shim saturation).

11. Large aperture insertion dipoles

11.1. Insertion dipole—100 mm

These magnets [54], termed D0, steer the beams into collision at the interaction points. Although each contains only a single beam, the increased aperture is required to accommodate the large beam size due to the low-beta configuration, the variations in beam crossing angles, and aperture required for collisions between unequal species.

Table 20
Summary of integral field quality data in 130 mm aperture insertion quadrupoles

Harmonic at 40 mm	Mean at 5 kA			Standard deviation at 5 kA		
	Q1 (1.44 m) (26 magnets)	Q2 (3.4 m) (27 magnets)	Q3 (2.1 m) (13 magnets)	Q1 (1.44 m) (26 magnets)	Q2 (3.4 m) (27 magnets)	Q3 (2.1 m) (13 magnets)
ITF(T/kA)	13.658	32.170	19.954	0.32%	0.13%	0.06%
b_2	0.14	−0.08	0.01	0.44	0.43	0.73
b_3	−0.14	−1.24	−0.34	0.44	0.19	0.51
b_4	0.02	0.08	−0.23	0.25	0.22	0.23
b_5	2.15	0.53	1.67	0.59	0.38	0.13
b_6	0.03	0.02	0.07	0.22	0.19	0.17
b_7	−0.14	−0.14	0.00	0.18	0.09	0.13
b_8	0.02	0.00	0.05	0.05	0.05	0.06
b_9	−0.10	−0.37	−0.31	0.17	0.07	0.03
b_{10}	0.00	0.00	0.00	0.02	0.02	0.01
a_2	−0.23	−0.18	0.40	0.56	0.51	0.59
a_3	−0.02	0.13	0.12	0.25	0.22	0.33
a_4	−0.08	0.05	0.06	0.29	0.28	0.15
a_5	−0.74	−0.09	−0.27	0.12	0.27	0.07
a_6	0.20	0.13	0.09	0.29	0.22	0.19
a_7	−0.04	−0.01	−0.01	0.08	0.10	0.07
a_8	−0.02	0.00	0.01	0.05	0.06	0.03
a_9	0.18	0.05	0.08	0.02	0.02	0.02
a_{10}	0.01	0.00	0.01	0.02	0.02	0.02

The mechanical construction is the same as that of the arc dipole. Even though the two D0 magnets on one side of the crossover are contained in a common cryostat, the corners of the containment vessels of the two yokes almost touch; in fact, this constrains the yoke outer diameter. A drawing of the cold mass is shown in Fig. 41.

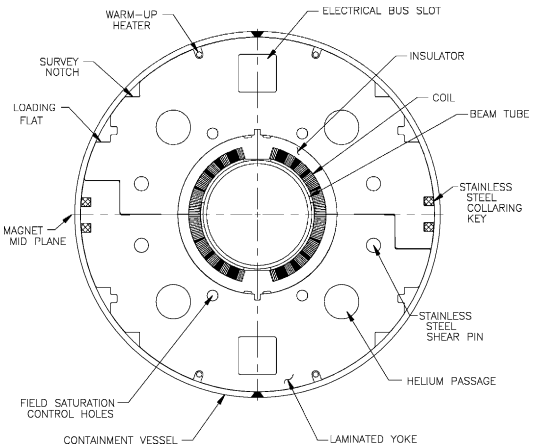

Fig. 41. Cross-section of the 100 mm D0 dipole magnet.

Table 21
Selected parameters of the 100 mm D0 dipole magnet

Parameter	Value
Field at top energy (T)	3.52
Current at top energy (kA)	5.0
Magnetic length (m)	3.6
Mechanical sagitta (mm)	7.6
Yoke outer diameter (mm)	310
Inductance (mH)	16.8
Stored energy (kJ)	210

The cable used is the same as that in the arc dipoles, see Tables 2 and 3. In order to achieve good field uniformity at low field, a single layer five-block coil design was needed. It has four symmetric wedges and a total of 40 turns in each half-coil. With the constraint on the yoke outer diameter mentioned above, it was necessary to limit the coil aperture to 100 mm. To maximize the effectiveness of this relatively small aperture, the D0 magnets were curved. Two types of D0, with opposite curvatures, were built to simplify interconnections. Some design parameters are given in Table 21.

Results of the quench tests of the D0 dipoles are shown in Fig. 42. Twelve of the 24 magnets had initial quenches below the 5 kA operating current, but all exceeded 5 kA on subsequent quenches. Later magnets were quenched only until they exceeded 6.5 kA (2–6 quenches), a 30% margin. Extra testing was done to verify that the magnets would not quench after a thermal cycle.

Field quality improvements were made in two steps, involving five magnets, before the final configuration of coil and yoke was achieved [54]. As it was for the insertion quadrupoles, the focus was on the D0 field quality at 5 kA. The critical

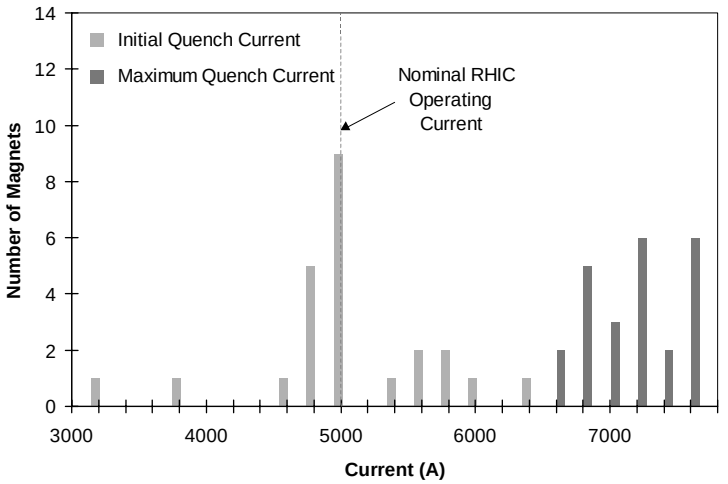

Fig. 42. Quench performance of 24 large aperture (100 mm) dipoles, tested at 4.5 K.

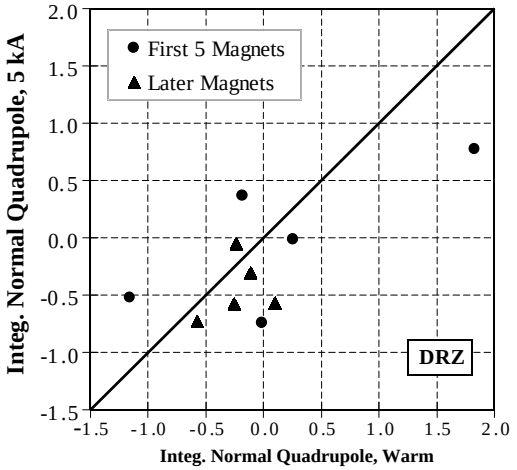

Fig. 43. Warm–cold correlation of the normal quadrupole harmonic (b_1) in D0 dipoles.

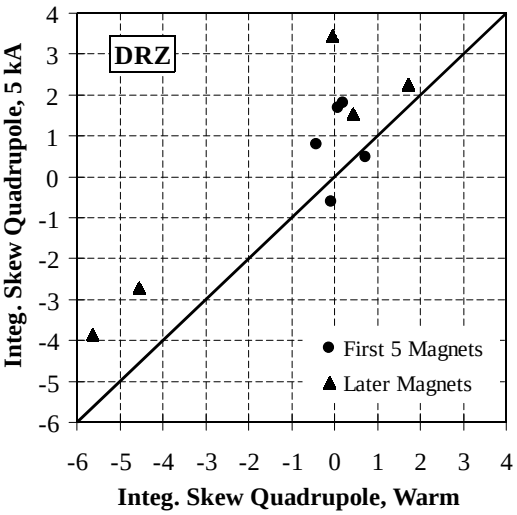

Fig. 44. Warm–cold correlation of the skew quadrupole harmonic (a_1) in D0 dipoles.

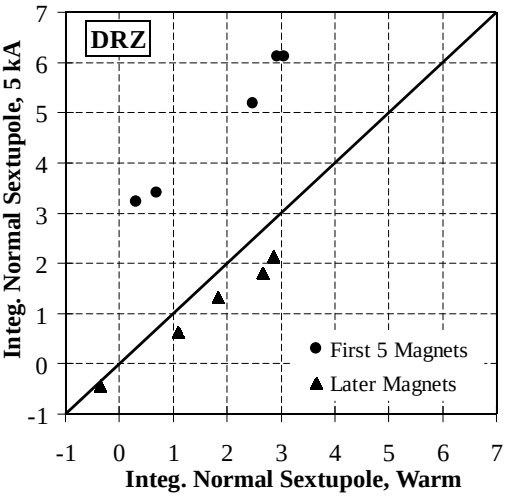

Fig. 45. Warm–cold correlation of the normal sextupole harmonic (b_2) in D0 dipoles.

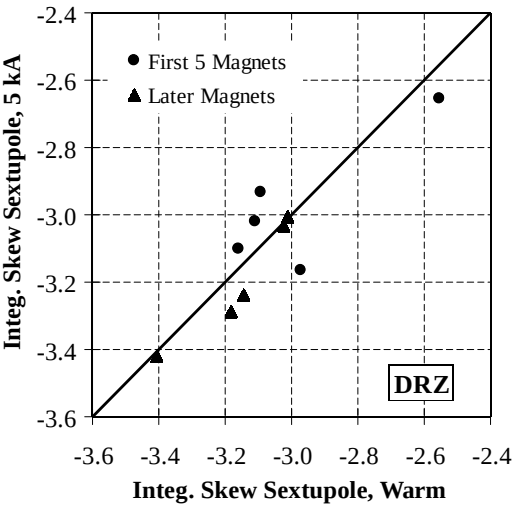

Fig. 46. Warm–cold correlation of the skew sextupole harmonic (a_2) in D0 dipoles.

data for this work, plots showing the correlation of warm and 5 kA measurements of the low order harmonics, are shown in Figs. 43–47. Fig. 45 shows the reduction in normal sextupole. As a consequence of the changes made to reduce the sextupole, the normal decapole saturation increased (Fig. 47). The remaining harmonics were unaffected. Because of the good warm–cold correlation of the harmonics, it was not necessary to measure the integral harmonics on all the D0's at 5 kA. Warm and cold integral data from the four magnets made in the final configuration were used to predict the integral 5 kA harmonics in the remaining magnets. (Cold measurements of the harmonics of a 1 m length in the middle of the magnet were made on an additional 17 D0's as a check of magnetization and saturation behavior.) Table 22 gives the warm integral harmonics for all 24 magnets installed in RHIC.

11.2. Insertion dipole—180 mm

Large aperture magnets named DX [55,56] are located immediately on either side of the interaction points. Both beams pass through each of these magnets, and their strength determines the collision angle. The spacing between the two beams at the end of the magnet away from the intersection determines the aperture required. The coil diameter of 180 mm ensures adequate field uniformity in the case of asymmetric operation, but requires that the dipole be moved sideways to accommodate the beam trajectories for some machine operating modes. The restricted axial space available in the lattice necessitates a somewhat higher field, 4.3 T, than is needed for the arc dipoles. To achieve this field with an adequate margin in a single layer coil, a wider cable was used. Fig. 48 shows a cross-section of this cold mass.

The coil is wound with 70 turns of 36-strand cable similar to that used in the 130 mm aperture insertion quadrupoles. It differs only in the keystone angle of 0.6° versus 1.0° in the cable for the quadrupoles, see Tables 2 and 3. A six-block coil

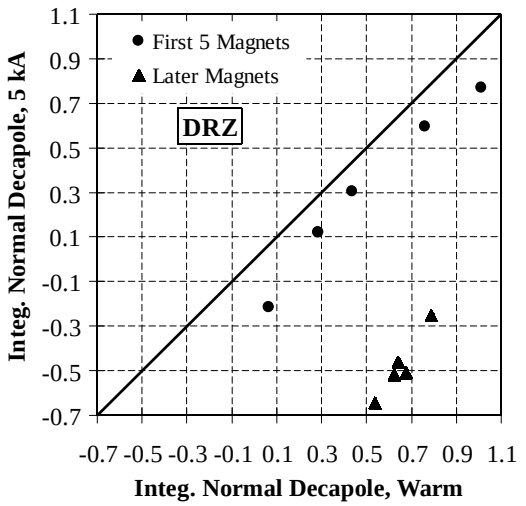

Fig. 47. Warm–cold correlation of the normal decapole harmonic (b_4) in D0 dipoles.

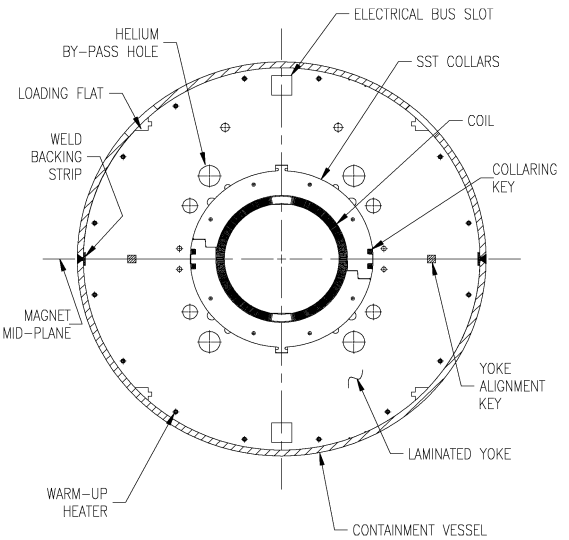

Fig. 48. Cross-section of the 180 mm DX dipole magnet.

Table 22

Summary of integral field quality (warm) in D0 dipoles

Harmonic at 31 mm	Mean (24 magnets)	Std. deviation. (24 magnets)	Harmonic at 31 mm	Mean (24 magnets)	Std. deviation (24 magnets)
b_1	0.00	0.57	a_1	−0.64	2.03
b_2	2.33	1.27	a_2	−3.24	0.29
b_3	−0.03	0.12	a_3	0.00	0.46
b_4	0.65	0.24	a_4	0.48	0.04
b_5	0.01	0.03	a_5	0.03	0.13
b_6	0.22	0.07	a_6	−0.25	0.01
b_7	0.00	0.01	a_7	0.01	0.03
b_8	−0.01	0.02	a_8	0.04	0.01
b_9	0.00	0.00	a_9	0.00	0.01
b_{10}	−0.12	0.01	a_{10}	−0.02	0.00

design was needed to achieve good field uniformity at low field; all five wedges are mechanically symmetric. To minimize unwanted harmonics in the ends, they were designed with frequent and sizable Ultem spacers, a feature that lead to a weak mechanical structure and possibly the observed erratic quench performance [57] (the quench performance of the one prototype that was built was improved by adding radial support to the inner radius of the coil ends [56]). Unlike all of the other RHIC magnets, this magnet was designed with stainless steel (Kawasaki high-Mn KHMN) collars to apply pre-stress to the coils. This was necessary because the forces in this large aperture magnet exceed those that could be tolerated by the yoke acting as collar. To minimize deflections and thus aid in assembly, a 40.1 mm wide collar was used. Iron saturation is controlled by a series of holes in the iron, near and at the yoke inner radius. The magnet is considered to be part of the blue ring for cryogenic purposes. The bus cutout is the same size as in the arc magnets, but the helium flow channel is slightly larger (3.175 cm) to assist in the control of iron saturation; there is an additional, smaller hole solely for saturation control. Because of the rather large stored energy and the modest ratio of copper to superconductor in the cable, which could result in a damaging hot spot temperature, active protection consisting of quench detection and firing of heaters to propagate the quench of the coil was incorporated. A diode was also installed across each of the two coils. Table 23 lists several of the design parameters.

Table 23
Selected parameters of the 180 mm DX dipole magnet

Field at top energy (T)	4.3
Current at top energy (kA)	6.6
Magnetic length (m)	3.7
Yoke outer diameter (mm)	622
Inductance (mH)	49
Stored energy (kJ)	1100

The quench performance of the 12 DX's installed in RHIC is summarized in Fig. 49. The dipoles required between one and three quenches to reach operating current. All were trained to at least 10% above the operating current of 6.6 kA. After installation in RHIC, six of the magnets required one quench each to reach operating current after the first cool-down, in agreement with the thermal cycle data obtained during production.

Warm integral measurements were made on all 13 magnets. The mean value of the transfer function was 2.5053 T m/kA with rms variation of 0.03%. Measurements of the integral transfer function and the first two allowed harmonics versus current are shown for a representative magnet in Figs. 50–52. Cold measurements of the

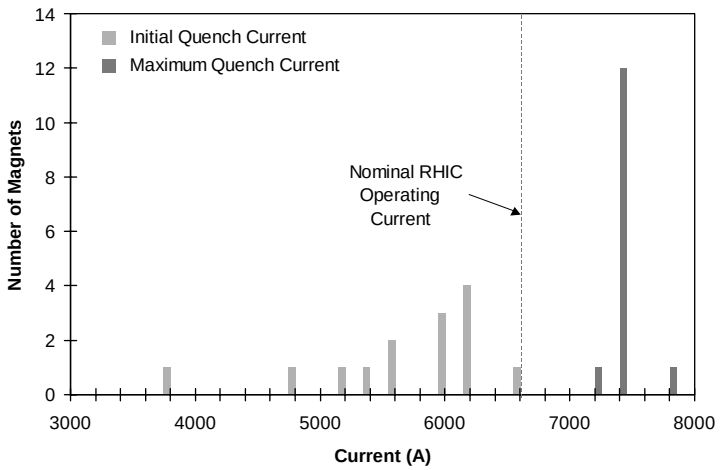

Fig. 49. Quench performance of 14 large aperture (180 mm) dipoles, tested at 4.5 K.

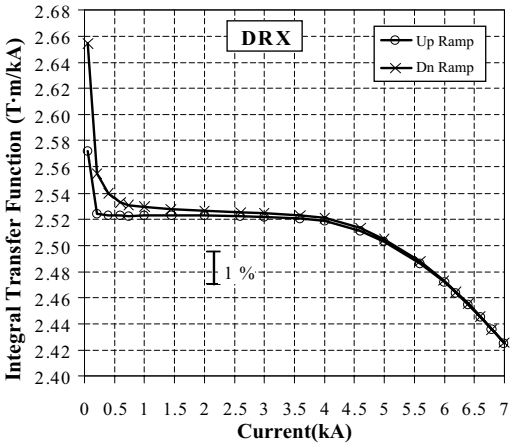

Fig. 50. Integral transfer function in DRX110.

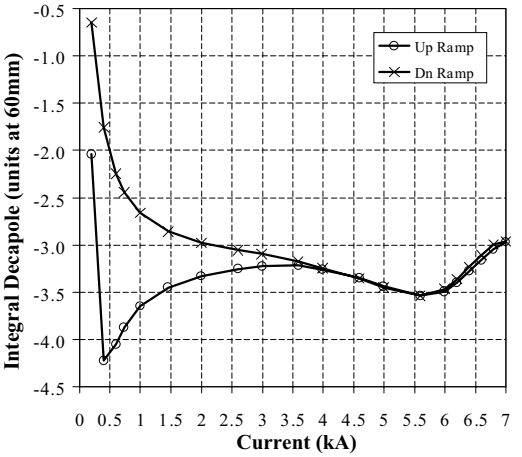

Fig. 52. Integral normal decapole harmonic in DRX110.

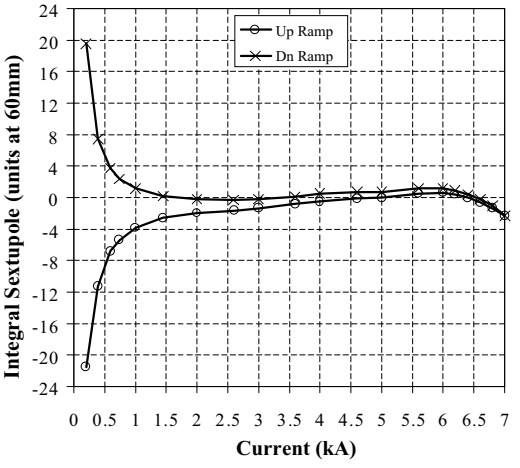

Fig. 51. Integral normal sextupole harmonic in DRX110.

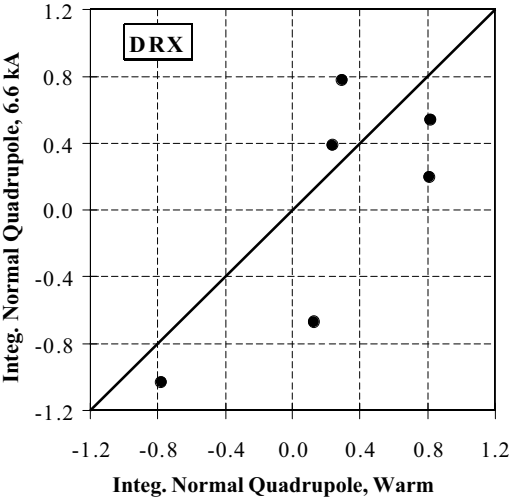

Fig. 53. Warm–cold correlation of b_1 in DRX magnets.

harmonics were made on all the magnets, but integral measurements were made on only six. Warm–cold correlations were used to estimate integral values for the remaining six. Warm–cold correlations for several low order terms are shown in Figs. 53–54. The field quality data for warm and cold measurements are given in Table 24.

12. Helical magnets

Helical magnets control the spin of the polarized protons in RHIC. The basic construction unit is a superconducting magnet producing a 4 T dipole field that rotates through 360° in a length of 2.4 m [58,59]. These magnets are assembled in groups of four to build four Snakes that control spin in the lattice and eight Rotators that orient spin axially at two collision points. Thus, the complete program requires 48 magnets. As of Spring 2001, nearly half of the magnets had been completed and construction of the rest was underway.

A cross-section drawing of the helical magnet is shown in Fig. 55. Parameters for the magnets are given in Table 25. Because multiple current leads exit each cryostat, a low current design (320A) was

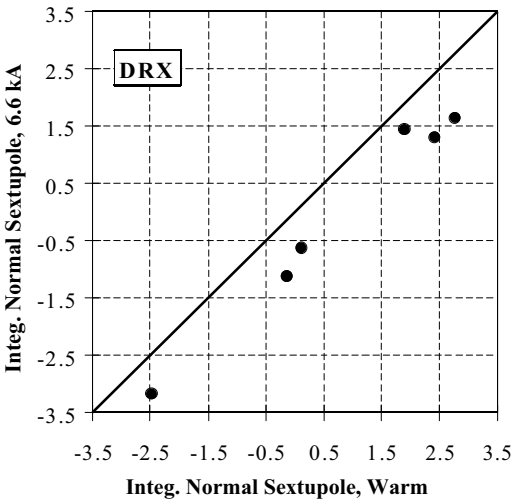

Fig. 54. Warm–cold correlation of b_2 in DRX magnets.

Table 24
Summary of integral field quality in DX dipoles

Harmonic at 60 mm	Mean		Standard deviation	
	30 A (13 magnets)	6600 A (6 magnets)	30 A (13 magnets)	6600 A (6 magnets)
b_1	0.04	0.03	0.63	0.72
b_2	0.53	−0.09	2.09	1.90
b_3	0.00	−0.03	0.19	0.22
b_4	−2.68	−2.95	0.57	0.41
b_5	0.03	−0.05	0.10	0.15
b_6	−1.91	−1.76	0.17	0.12
b_7	0.01	0.01	0.04	0.06
b_8	−1.09	−1.15	0.07	0.07
b_9	0.00	0.01	0.02	0.02
b_{10}	−1.13	−1.15	0.02	0.02
a_1	−1.00	−2.33	2.37	0.96
a_2	−2.54	−2.70	0.53	0.32
a_3	0.38	−0.06	0.99	1.10
a_4	0.30	0.34	0.25	0.16
a_5	0.34	0.19	0.37	0.38
a_6	−0.21	−0.15	0.15	0.08
a_7	0.19	0.15	0.11	0.11
a_8	−0.04	−0.05	0.04	0.04
a_9	0.09	0.08	0.04	0.05
a_{10}	0.03	0.06	0.02	0.02

used to minimize the cryogenic load due to the leads. By the standards of superconducting magnets, the field quality requirements are relatively modest (harmonics $<10^{-3}$ of the main field). The error allowed on the rotation angle is 2°.

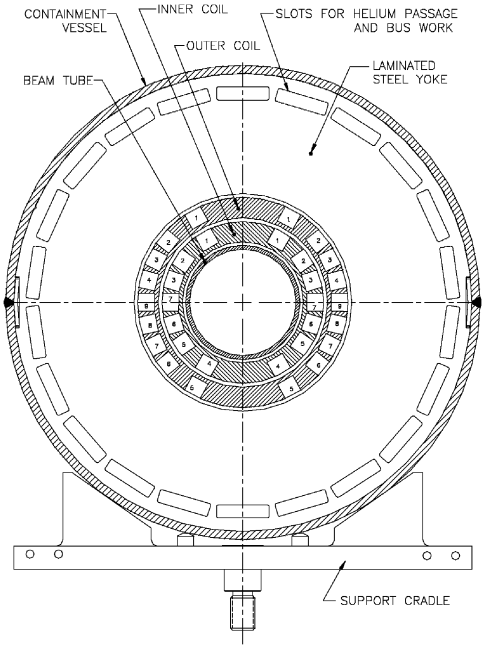

Fig. 55. Cross-section of the helical dipole magnet. The yoke OD is 356 mm. The innermost conductor is at an ID of 100 mm.

Table 25
Selected parameters of the RHIC helical dipole magnets

Parameter	Units	Value
Aperture	mm	100
Magnetic length	m	2.4
Field	T	4
Current	A	320
Number of turns		1680
Inductance	H	4.8
Stored energy at 4 T	kJ	240
Diameter of yoke	mm	355.6
Num. of strands in cable		7
Strand diameter	mm	0.33
Cu to non-Cu ratio		2.5:1

The coil structure consists of two aluminum tubes, each with slots as shown in Fig. 56. These are filled with Kapton-insulated superconducting cable. The tubes are surrounded by a yoke made of single piece, low-carbon steel laminations. Holes near the outer perimeter of the yoke allow for tie rods, warm-up heaters, passage of helium coolant, and bus work for magnet interconnections. The slots rotate along the length of the magnet but the

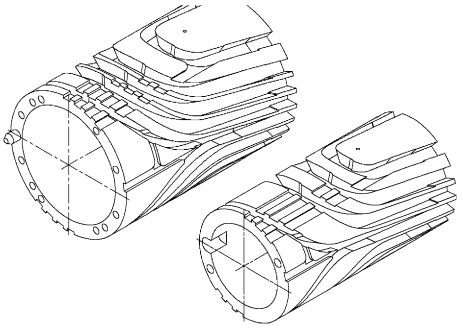

Fig. 56. Drawing of the coil tube ends. End Lorentz forces are contained in the slots.

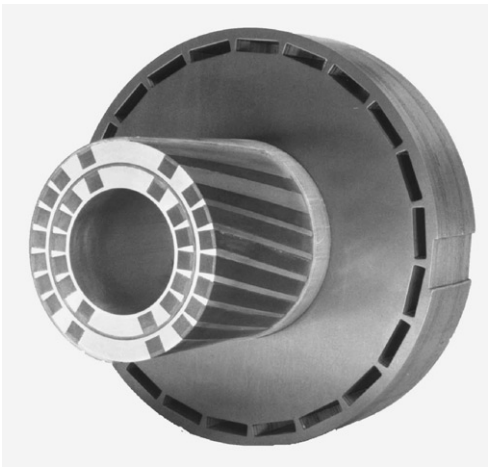

Fig. 57. Photograph of a section cut from a prototype helical magnet.

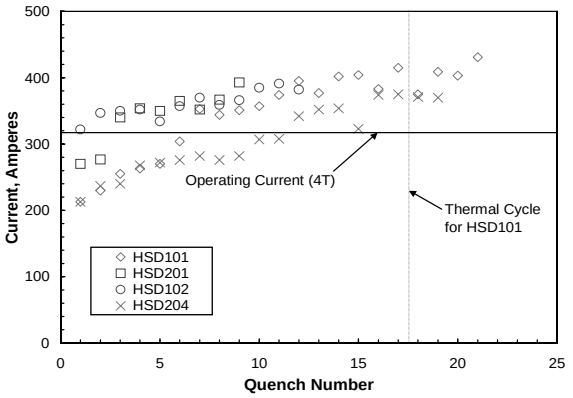

Fig. 58. Quench performance of the four magnets of the first Snake. After some initial training, each reached a current comfortably above the maximum operating point of 4 T. A thermal cycle showed no retraining.

holes in the yoke do not, so the yoke laminations were designed with rotational symmetry in mind. Azimuthal Lorentz forces are contained in the individual slots. The outward Lorentz forces are ultimately contained by the single piece yoke. In the ends, the difficult Lorentz force problem is again solved by containing the forces in the individual slots.

The superconducting cable is placed by hand and without tension into the slots in an ordered array. The width in the slots is such that 12 turns of the round cable, which is about 1.1 mm in diameter, have an average of 25 μm space between turns. A layer of B-stage fiberglass/epoxy with adhesive film on each side is placed between each layer. After winding, press plates of 3.1 mm thick G10 are applied to each slot. A Kevlar wrap is then applied to the tube under tension. In the subsequent curing operation, the stretch in the Kevlar allows the press plates to move radially inward without losing all tension, thereby compressing the windings and removing voids in the slots as the epoxy softens and fills the remaining spaces. Helium is still able to penetrate this package and fill the $\sim$10% free space inside the Kapton wrap and around the wires of the cable. At the ends of the magnet, space is left in the slots to accommodate the axial growth of the coil during curing. Voids remaining in the ends after curing are filled with epoxy by hand. After curing, the Kevlar is removed so that the leads can be secured. The coil is then wrapped with fiberglass cloth, Kevlar under tension, and Tedlar. (The Tedlar prevents epoxy in the next layer from seeping into the Kevlar). Multiple layers of fiberglass cloth and epoxy are applied to build the radial thickness needed for the final step, machining the cylinder to a precise radius ($\sim$50 μm). The epoxy cures at room temperature.

The two coils are assembled, aligned, pinned together, and bolted to a plate that serves as the primary alignment reference of the magnet. The laminations are weighed before assembly to the coils. The length of the yoke is set by tie bars. The tie bars and coils are held on a plate at only

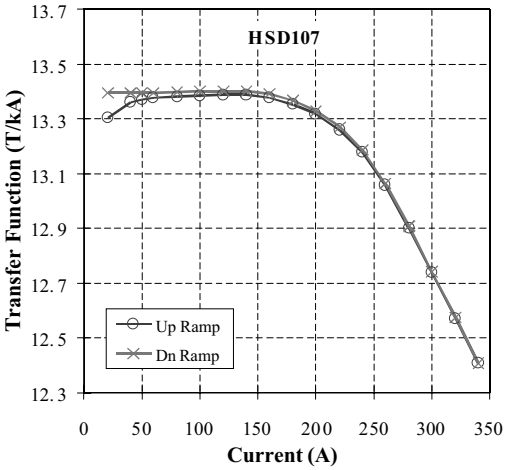

Fig. 59. Transfer function at the center of HSD107.

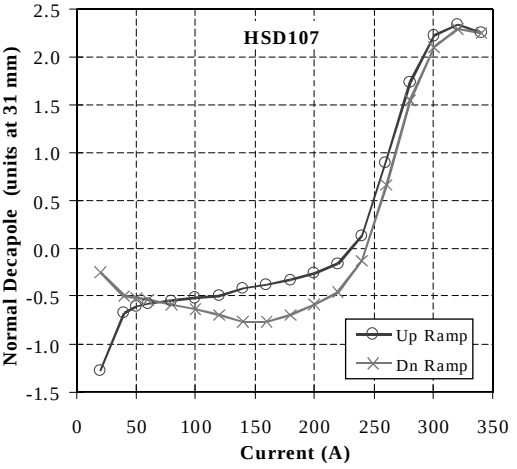

Fig. 61. Normal decapole harmonic at the center of HSD107.

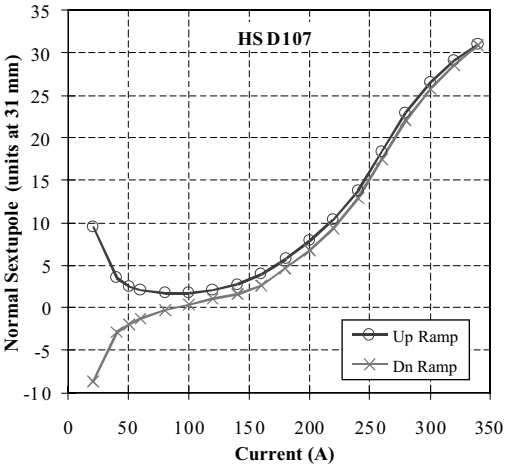

Fig. 60. Normal sextupole harmonic at the center of HSD107.

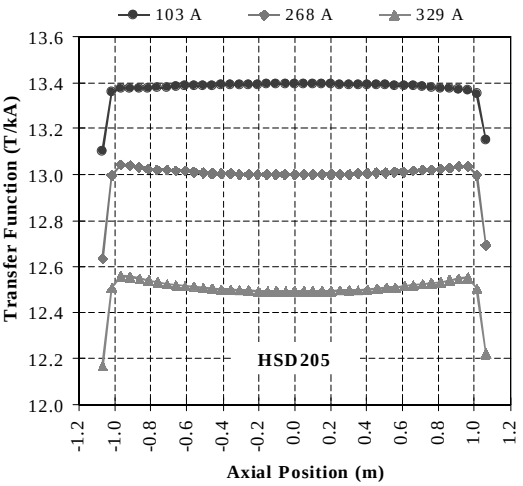

Fig. 62. Axial scan of the transfer function in HSD205.

the lead end of the coils. Thus, the coils can follow the contraction of the aluminum tube during cooldown. Fig. 57 shows a section cut from a prototype helical magnet [60].

Each of the individual windings is connected in a series connection on a circuit board at the end of the magnet. A 50 mΩ resistor is connected across each of the windings to avoid overheating during a quench. The large inductance of the windings (0.3 H on average) and the 50 mΩ parallel resistance lead to an indeterminate field in the magnet when it is ramped. This is acceptable because the magnet is required to be operated only in a DC mode or with very slow (<1 A/s) ramp rates.

The magnets were tested individually in a vertical dewar filled with liquid helium. Quench test results from the magnets that were installed into the first Snake are shown in Fig. 58. Initially, magnets were trained to currents close to conductor limit, $\sim$410 A. The training was monotonic but sometimes slow at the highest currents. The test protocol later called for training the magnets to 360 A, about 10% above the maximum

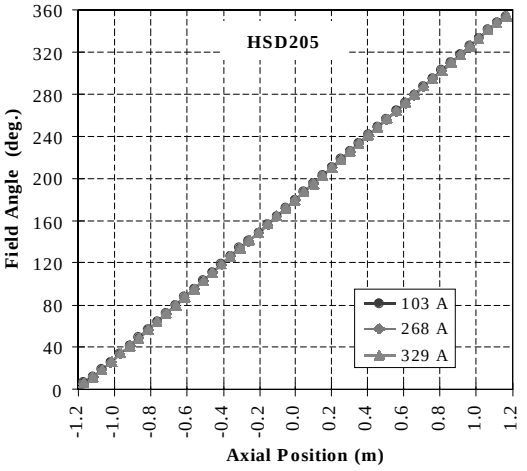

Fig. 63. Field angle as a function of the axial position in HSD205.

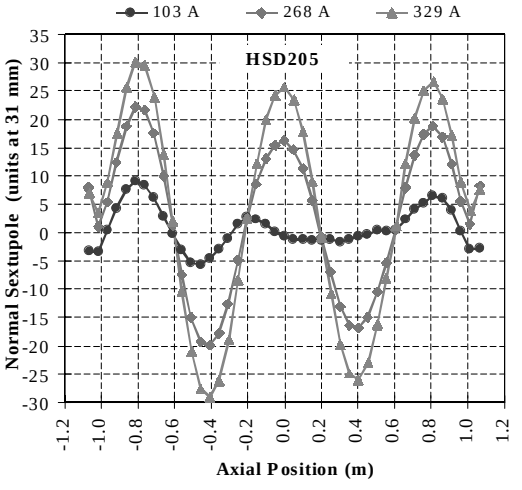

Fig. 64. Normal sextupole harmonic as a function of the axial position in HSD205.

operating current. Magnets have typically reached 360 A in a few quenches.

Ideally, the integral field of each helical magnet will be zero. The acceptance criterion calls for it to be small: $[(\int B_y(z)\,dz)^2 + (\int B_x(z)\,dz)^2]^{1/2} < 5 \times 10^{-2}$ T m. In terms of the rotation angle of the dipole field vector, this tolerance is $\sim 1.9^\circ$. The integral field is measured using a 3.57 m long, 48 mm diameter rotating coil. All magnets tested thus far have easily met this requirement.

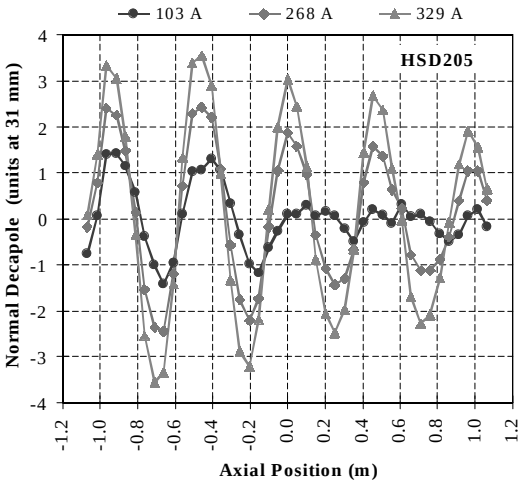

Fig. 65. Normal decapole harmonic as a function of the axial position in HSD205.

Helical magnets have axial fields in the magnet straight section. They can be expressed in cylindrical coordinates using Bessel functions as basis functions [61,62]. In these magnets the resulting harmonic coefficients are close to those for straight magnets; the harmonics measured with the short (51 mm) standard harmonic coil used require a correction of only a few percent. This coil has diameter 68 mm. Field quality measurements at the center of a typical magnet as a function of current are shown in Figs. 59–61. The decrease in the transfer function and the increase in the sextupole with current are caused by saturation of the steel yoke, which is undersized in order to limit the physical size of the magnet. Field quality measurements made by stepping the coil through the length of a magnet at three fixed currents are shown in Figs. 62–65.

References

[1] P. Thompson, J. Cottingham, P. Dahl, R. Fernow, M. Garber, A. Ghosh, C. Goodzeit, A. Greene, H. Hahn, J. Herrera, S. Kahn, E. Kelly, G. Morgan, S. Plate, A. Prodell, W. Sampson, W. Schneider, R. Shutt, P. Wanderer, E. Willen, Status of magnet system for RHIC, BNL-38459, Proceedings of the Second Conference on the Intersections between Particle and Nuclear Physics, Lake Louise, Canada, May 1986.

[2] E. Willen, Magnets for RHIC, BNL-38966, Proceedings of the ICFA Workshop on Superconducting Magnets and Cryogenics, Brookhaven National Laboratory, May 12–16, 1986.

[3] E. Willen, Superconducting Magnets, BNL-64183, Proceedings of the INFN Eloisatron Project 34th Workshop, "Hadron Collider at the Highest Energy and Luminosity", Erice, Sicily, November 4–13, 1996.

[4] A. Greene, M. Anerella, J. Cozzolino, J. Escallier, D. Fisher, G. Ganetis, A. Ghosh, R. Gupta, A. Jain, S. Kahn, E. Kelly, R. Lebel, G. Morgan, A. Morgillo, S. Mulhall, J. Muratore, S. Plate, A. Prodell, M. Rehak, W. Sampson, R. Thomas, P. Thompson, P. Wanderer, E. Willen, The magnet system of the Relativistic Heavy Ion Collider (RHIC), BNL-61790, Proceedings of the 14th International Conference on Magnet Technology, Tampere, Finland, June 11–16, 1995.

[5] P. Wanderer, Status of RHIC construction, Proceedings of the 15th International Conference on Magnet Technology, Beijing, China, October 20–24, 1997.

[6] M. Garber, A. Ghosh, A. Greene, D. McChesney, A. Morgillo, R. Shah, S. DelRe, G. Epstein, S. Hong, J. Lichtenwalner, P. O'Larey, D. Smathers, M. Boivin, R. Meserve, Superconducting wire and cable for RHIC, BNL-49321, Proceedings of the 13th International Conference on Magnet Technology, Vancouver, BC, Canada, September 20–24, 1993.

[7] A. Greene, M. Garber, A. Ghosh, D. McChesney, A. Morgillo, R. Shah, S. DelRe, G. Epstein, S. Hong, J. Lichtenwalner, P. O'Larey, D. Smathers, M. Boivin, R. Meserve, Manufacture and testing of the superconducting wire and cable for the RHIC dipoles and quadrupoles, BNL-60350, Proceedings of the 1994 Applied Superconductivity Conference, Boston, MA, October 16–21, 1994.

[8] A. Jain, G. Ganetis, J. Muratore, R. Thomas, P. Wanderer, Time decay, snap-back, and ramp rate effects in RHIC 8 cm dipoles and quadrupoles, Magnet Division Note 593, May 10, 2000.

[9] W. Fischer, A. Jain, S. Tepikian, Beam-based measurements of persistent current decay in RHIC, Brookhaven Magnet Division Note 600, January 5, 2001.

[10] P. Dahl, J. Cottingham, M. Garber, A. Ghosh, C. Goodzeit, A. Greene, J. Herrera, S. Kahn, E. Kelly, G. Morgan, A. Prodell, W. Sampson, W. Schneider, R. Shutt, P. Thompson, P. Wanderer, E. Willen, Performance of initial full-length RHIC dipoles, BNL-40545, Proceedings of the Tenth International Conference on Magnet Technology, Boston, MA, September 21–25, 1987.

[11] P. Thompson, R. Gupta, S. Kahn, H. Hahn, G. Morgan, P. Wanderer, E. Willen, Revised cross-section for RHIC dipole magnets, BNL-45721, Proceedings of the 1991 Particle Accelerator Conference, San Francisco, CA, May 6–9, 1991.

[12] M. Anerella, A. Ghosh, E. Kelly, J. Schmalzle, E. Willen, Improved cable insulation for superconducting magnets, Proceedings of the 1993 Particle Accelerator Conference, Washington, DC, May 17–20, 1993.

[13] S. Kahn, R. Gupta, A. Jain, G. Morgan, P. Thompson, Calculations of magnetic field for the end design of the RHIC arc dipole, Proceedings of the 1993 Particle Accelerator Conference, Washington, DC, May 17–20, 1993.

[14] G. Morgan, A. Morgillo, K. Power, P. Thompson, New coil end design for the RHIC arc dipole, BNL-49324, Proceedings of the 13th International Conference on Magnet Technology, Vancouver, BC, Canada, September 1993.

[15] R. Gupta, A. Jain, S. Kahn, G. Morgan, P. Thompson, P. Wanderer, E. Willen, Field quality improvements in superconducting magnets for RHIC, European Particle Accelerator Conference 94, London, UK, pp. 2928–2930.

[16] M. Rehak, R. Shutt, Pressure drops and temperature increases in RHIC magnets, Brookhaven Magnet Division Note 423, March 4, 1992.

[17] C. Goodzeit, M. Anerella, G. Ganetis, Measurement of internal forces in superconducting accelerator magnets with strain gauge transducers, Proceedings of the 1988 Applied Superconductivity Conference, San Francisco, CA, August 21–25, 1988.

[18] G. Morgan, Final report of the task force on the RHIC iron specification, Brookhaven Magnet Division Note 420, February 26, 1992.

[19] R. Thomas, G. Morgan, Measurements of magnetic permeability and H_c of magnet steels using digital techniques, BNL-47851, Presentation at the 11th Annual Conference on Properties and Applications of Magnetic Materials, Chicago, IL, May 12–14, 1992.

[20] G. Morgan, A B-H table for the Kawasaki iron used in the RHIC arc dipoles, Brookhaven Magnet Division Note 535, May 13, 1994.

[21] A. Jain, R. Gupta, P. Thompson, P. Wanderer, Skew quadrupole in RHIC dipole magnets at high fields, BNL-61362, Proceedings of the 14th International Conference on Magnet Technology, Tampere, Finland, June 11–16, 1995.

[22] J. Muratore, M. Anerella, G. Ganetis, M. Garber, A. Ghosh, A. Greene, R. Gupta, A. Jain, S. Kahn, E. Kelly, G. Morgan, A. Prodell, M. Rehak, E.P. Rohrer, W. Sampson, R. Shutt, R. Thomas, P. Thompson, P. Wanderer, E. Willen, Quench propagation study for full-length RHIC dipole magnets, BNL-49323, Proceedings of the 13th International Conference on Magnet Technology, Vancouver, BC, Canada, September 20–24, 1993.

[23] J. Sondericker, L. Wolf, Alternative concepts for structurally supporting the cold mass of a superconducting accelerator magnet, Proceedings of the Third Annual International Industrial Symposium on the SuperCollider (IISSC), Atlanta, GA, March 13–15, 1991.

[24] P. Wanderer, M. Anerella, A. Greene, E. Kelly, E. Willen, Nucl. Instr. and Meth. B 99 (1995) 7.

[25] M. Anerella, D. Fisher, E. Sheedy, T. McGuire, Industrial production of RHIC magnets, BNL-61361, Proceedings of

the 14th International Conference on Magnet Technology, Tampere, Finland, June 11–16, 1995.

[26] D. Fisher, M. Anerella, P. Wanderer, Successful partnership between Brookhaven National Laboratory and Northrop Grumman Corp. for Construction of RHIC superconducting magnets, Proceedings of the 16th International Conference on Magnet Technology, Ponte Vedra Beach, FL, September 26–October 2, 1999.

[27] R. Gupta, A. Jain, S. Kahn, G. Morgan, P. Thompson, P. Wanderer, E. Willen, Field quality control through the production phase of RHIC arc dipoles, BNL-61226, Proceedings of the 1995 Particle Accelerator Conference and International Conference on High Energy Accelerators, Dallas, TX, May 1–5, 1995.

[28] P. Wanderer, Magnet measurements for series production, CERN Accelerator School, Measurement and Alignment of Accelerator & Detector Magnets, CERN Report, CERN 98-05 August 4, 1998.

[29] J. Wei, R. Gupta, A. Jain, S. Peggs, C.G. Trahern, D. Trbojevic, P. Wanderer, Field quality evaluation of the superconducting magnets of the relativistic heavy ion collider, Proceedings of the 1995 Particle Accelerator Conference, Dallas, TX, May 1–5, 1995, p. 461.

[30] W. Fischer, A. Jain, S. Tepikian, Phys. Rev. Special Topics, 4 (2001) 041002.

[31] P. Thompson, G. Cottingham, M. Garber, A. Ghosh, C. Goodzeit, A. Greene, J. Herrera, S. Kahn, E. Kelly, G. Morgan, S. Plate, A. Prodell, W. Sampson, W. Schneider, R. Shutt, P. Wanderer, E. Willen, Status of the quadrupoles for RHIC, BNL-41899, Proceedings of the 1989 Particle Accelerator Conference, Chicago, IL, March 20–23, 1989.

[32] P. Thompson, M. Anerella, G. Ganetis, M. Garber, A. Ghosh, A. Greene, R. Gupta, A. Jain, S. Kahn, G. Morgan, A. Morgillo, J. Muratore, A. Prodell, M. Rehak, W. Sampson, P. Wanderer, E. Willen, "B" Series RHIC arc quadrupoles, Proceedings of the 1993 Particle Accelerator Conference, Washington, DC, May 17–20, 1993.

[33] P. Wanderer, M. Anerella, G. Ganetis, M. Garber, A. Ghosh, A. Greene, R. Gupta, A. Jain, S. Kahn, E. Kelly, G. Morgan, J. Muratore, A. Prodell, M. Rehak, E.P. Rohrer, W. Sampson, R. Shutt, R. Thomas, P. Thompson, E. Willen, Test of eight superconducting arc quadrupoles for RHIC, BNL-49348, Proceedings of the 13th International Conference on Magnet Technology, Vancouver, BC, Canada, September 20–24, 1993.

[34] P. Thompson, M. Anerella, G. Ganetis, A. Ghosh, A. Greene, R. Gupta, A. Jain, E. Kelly, M. Lindner, G. Morgan, J. Muratore, W. Sampson, P. Wanderer, E. Willen, Superconducting sextupoles and trim quadrupoles for RHIC, BNL-61224, Proceedings of the 1995 Particle Accelerator Conference and International Conference on High Energy Accelerators, Dallas, TX, May 1–5, 1995.

[35] P. Wanderer, M. Anerella, J. Cottingham, G. Ganetis, M. Garber, A. Ghosh, C. Goodzeit, A. Greene, R. Gupta, J. Herrera, S. Kahn, E. Kelly, A. Meade, G. Morgan, J. Muratore, A. Prodell, M. Rehak, E.P. Rohrer, W. Sampson, R. Shutt, J. Skaritka, P. Thompson, E. Willen, Performance of trim coils made by a novel method, BNL-45720, Proceedings of the 12th International Conference on Magnet Technology, Leningrad, USSR, June 24–28, 1991.

[36] A. Morgillo, J. Escallier, G. Ganetis, A. Greene, A. Ghosh, A. Jain, E. Kelly, A. Marone, G. Morgan, J. Muratore, W. Sampson, P. Thompson, P. Wanderer, E. Willen, Superconducting 8 cm corrector magnets for the relativistic heavy ion collider (RHIC), BNL-61264, Proceedings of the 1995 Particle Accelerator Conference and International Conference on High Energy Accelerators, Dallas, TX, May 1–5, 1995.

[37] J. Muratore, A. Jain, G. Ganetis, A. Ghosh, A. Marone, A. Morgillo, W. Sampson, P. Thompson, P. Wanderer, Results from the completed production run of superconducting corrector magnets for RHIC, Proceedings of the 1997 Particle Accelerator Conference, Vancouver, BC, pp. 3353–3355.

[38] S. Mulhall, H. Foelsche, G. Ganetis, A. Greene, E. Kelly, S. Plate, E. Willen, Combined element magnet production for the relativistic heavy ion collider (RHIC) at BNL, BNL-61234, Proceedings of the 1995 Particle Accelerator Conference and International Conference on High Energy Accelerators, Dallas, TX, May 1–5, 1995.

[39] R. Shutt, K. Hornik, M. Rehak, Corrector-quadrupole-sextupole (CQS) power leads for the relativistic heavy ion collider (RHIC) at Brookhaven National Laboratory (BNL), Proceedings of the Fifth Annual International Industrial Symposium on the SuperCollider (IISSC), San Francisco, CA, May 6–8, 1993.

[40] M. Goldman, R. Sikora, T. Shea, Preliminary studies on a magneto-optical procedure for aligning RHIC magnets, Proceedings of the 1993 Particle Accelerator Conference, Washington, DC, May 17–20, 1993.

[41] D. Trbojevic, P. Cameron, G. Ganetis, M. Goldman, R. Gupta, M. Harrison, M. Hemmer, F. Karl, A. Jain, W. Louie, S. Mulhall, S. Peggs, S. Tepikian, R. Thomas, P. Wanderer, Alignment and survey of the elements in RHIC, Proceedings of the 1995 Particle Accelerator Conference and International Conference on High Energy Accelerators, Dallas, TX, May 1–5, 1995.

[42] A. Jain, A "survey antenna" for determining magnetic center, Presented at the Tenth International Magnet Measurement Workshop (IMMW-10), FNAL, Batavia, IL, October 13–16, 1997.

[43] J. Cozzolino, M. Anerella, A. Jain, W. Louie, J. Muratore, P. Wanderer, Removal of axial twist in RHIC insertion quadrupole magnets, Proceedings of the 1997 Particle Accelerator Conference, Vancouver, Canada, May 1997.

[44] R. Shutt, M. Rehak, Instabilities of bellows: dependence on internal pressure, end supports, and interactions in accelerator magnet systems, BNL-44548, Proceedings of the 1990 American Society of Mechanical Engineers (ASME) Winter Annual Meeting (WAM), Dallas, TX, November 25–30, 1990.

[45] R. Shutt, M. Rehak, Stability of bellows used as expansion joints between superconducting magnets in accelerators, BNL-45337, Proceedings of the Third Annual International Industrial Symposium on the SuperCollider (IISSC), Atlanta, GA, March 13–15, 1991.

[46] J. Wei, G. Ganetis, R. Gupta, M. Harrison, M. Hemmer, A. Jain, F. Karl, S. Peggs, S. Tepikian, P.A. Thompson, D. Trbojevic, P. Wanderer, Misalignment evaluation of superconducting magnets in the relativistic heavy ion collider, Proceedings of the Fifth European Particle Accelerator Conference, Sitges, Barcelona, June 10–14, 1996, pp. 2222–2224.

[47] A. Jain, M. Anerella, J. Escallier, G. Ganetis, A. Ghosh, R. Gupta, E. Kelly, A. Marone, G. Morgan, J. Muratore, A. Prodell, W. Sampson, R. Thomas, P. Thompson, P. Wanderer, E. Willen, Superconducting 13 cm corrector magnets for the relativistic heavy ion collider (RHIC), Proceedings of the 16th International Conference on Magnet Technology, Ponte Vedra Beach, FL, September 12–October 2, 1999.

[48] R. Gupta, M. Anerella, G. Ganetis, M. Garber, A. Ghosh, A. Greene, A. Jain, S. Kahn, E. Kelly, E. Killian, G. Morgan, A. Morgillo, J. Muratore, A. Prodell, M. Rehak, W. Sampson, R. Shutt, P. Thompson, P. Wanderer, E. Willen, Large aperture quadrupoles for RHIC interaction regions, Proceedings of the 1993 Particle Accelerator Conference, Washington, DC, May 17–20, 1993.

[49] R. Gupta, M. Anerella, J. Cozzolino, B. Erickson, A. Greene, A. Jain, S. Kahn, E. Kelly, G. Morgan, P. Thompson, P. Wanderer, E. Willen, Tuning shims for high field quality in superconducting magnets, BNL-61106, Proceedings of the 14th International Conference on Magnet Technology, Tampere, Finland, June 11–16, 1995.

[50] T. Ogitsu, A. Terashima, K. Tsuchiya, G. Ganetis, J. Muratore, P. Wanderer, IEEE Trans. Magn. 32 (4) (1996) 21.

[51] R. Gupta, M.Anerella, J. Cozzolino, A. Ghosh, A. Jain, S. Kahn, E. Kelly, G. Morgan, J. Muratore, A. Prodell, W. Sampson, P. Thompson, P. Wanderer, E. Willen, RHIC IR quadrupoles and field quality state of the art in superconducting accelerator magnets, Proceedings of the 1999 Particle Accelerator Conference, New York, 1999, p. 185.

[52] R. Gupta, A. Jain, J. Muratore, P. Wanderer, E. Willen, C. Wyss, Change in field harmonics after quench and thermal cycles in superconducting magnets, Proceedings of the 1997 Particle Accelerator Conference, Vancouver, BC, p. 3347.

[53] J. Wei, R. Gupta, M. Harrison, A. Jain, S. Peggs, P. Thompson, D. Trbojevic, P. Wanderer, Real-world sorting of RHIC superconducting magnets, Proceedings of the 1999 Particle Accelerator Conference, New York, 1999, p. 3176.

[54] J. Schmalzle, M. Anerella, G. Ganetis, A. Ghosh, R. Gupta, A. Jain, S. Kahn, G. Morgan, J. Muratore, W. Sampson, P. Wanderer, E. Willen, RHIC D0 insertion dipole design iterations during production, Proceedings of the 1997 Particle Accelerator Conference, Vancouver, Canada, May 12–16, 1997.

[55] G. Morgan, Design of the large aperture superconducting magnet DX, BNL-61425, Proceedings of the Conference on the Computation of the Electromagnetic Fields Compumag, Berlin, Germany, July 10–13, 1995.

[56] J. Schmalzle, M. Anerella, G. Ganetis, A. Jain, G. Morgan, J. Muratore, P. Wanderer, RHIC DX dipole magnet construction, Proceedings of the 16th International Conference on Magnet Technology, Ponte Vedra Beach, FL, September 26–October 2, 1999.

[57] A. Jain, J. Muratore, M. Anerella, G. Ganetis, A. Marone, G. Morgan, A. Prodell, J. Schmalzle, R. Thomas, P. Wanderer, Quench performance and field quality of DX dipoles for RHIC, Proceedings of the 1999 Particle Accelerator Conference, New York, NY, March 29–April 2, 1999.

[58] E. Willen, R. Gupta, A. Jain, E. Kelly, G. Morgan, J. Muratore, R. Thomas, A helical magnet design for RHIC, Proceedings of the 1997 Particle Accelerator Conference, Vancouver, Canada, May 1997.

[59] E. Willen, E. Kelly, M. Anerella, J. Escallier, G. Ganetis, A. Ghosh, R. Gupta, A. Jain, A. Marone, G. Morgan, J. Muratore, A. Prodell, P. Wanderer, M. Okamura, Construction of helical magnets for RHIC, Proceedings of the 1999 Particle Accelerator Conference, New York, 1999, p. 3161.

[60] M. Okamura, T. Tominaka, T. Kawaguchi, T. Katayama, A. Jain, J. Muratore, G. Morgan, E. Willen, Nucl. Instr. and Meth. A 452 (2000) 53.

[61] W. Fischer, M. Okamura, Parameterization and measurements of helical magnetic fields, Proceedings of the 1997 Particle Accelerator Conference, Vancouver, Canada, May 1997.

[62] E. Willen, M. Anerella, J. Escallier, G. Ganetis, A. Ghosh, A. Jain, E. Kelly, G. Morgan, J. Muratore, A. Prodell, P. Wanderer, R. Gupta, M. Okamura, Performance of helical magnets for RHIC, Proceedings of the 16th International Conference on Magnet Technology, Ponte Vedra Beach, FL, September 12–October 2, 1999.